NASA/TM—2011-216946 AIAA–2010–7670

Experimental Observations on the Deformation and Breakup of Water Droplets Near the Leading Edge of an Airfoil

Mario Vargas
Glenn Research Center, Cleveland, Ohio

Alex Feo
Instituto Nacional de Técnica Aeroespacial, Madrid, Spain

January 2011

NASA STI Program . . . in Profile

Since its founding, NASA has been dedicated to the advancement of aeronautics and space science. The NASA Scientific and Technical Information (STI) program plays a key part in helping NASA maintain this important role.

The NASA STI Program operates under the auspices of the Agency Chief Information Officer. It collects, organizes, provides for archiving, and disseminates NASA's STI. The NASA STI program provides access to the NASA Aeronautics and Space Database and its public interface, the NASA Technical Reports Server, thus providing one of the largest collections of aeronautical and space science STI in the world. Results are published in both non-NASA channels and by NASA in the NASA STI Report Series, which includes the following report types:

- TECHNICAL PUBLICATION. Reports of completed research or a major significant phase of research that present the results of NASA programs and include extensive data or theoretical analysis. Includes compilations of significant scientific and technical data and information deemed to be of continuing reference value. NASA counterpart of peer-reviewed formal professional papers but has less stringent limitations on manuscript length and extent of graphic presentations.

- TECHNICAL MEMORANDUM. Scientific and technical findings that are preliminary or of specialized interest, e.g., quick release reports, working papers, and bibliographies that contain minimal annotation. Does not contain extensive analysis.

- CONTRACTOR REPORT. Scientific and technical findings by NASA-sponsored contractors and grantees.

- CONFERENCE PUBLICATION. Collected papers from scientific and technical conferences, symposia, seminars, or other meetings sponsored or cosponsored by NASA.

- SPECIAL PUBLICATION. Scientific, technical, or historical information from NASA programs, projects, and missions, often concerned with subjects having substantial public interest.

- TECHNICAL TRANSLATION. English-language translations of foreign scientific and technical material pertinent to NASA's mission.

Specialized services also include creating custom thesauri, building customized databases, organizing and publishing research results.

For more information about the NASA STI program, see the following:

- Access the NASA STI program home page at *http://www.sti.nasa.gov*

- E-mail your question via the Internet to *help@sti.nasa.gov*

- Fax your question to the NASA STI Help Desk at 443–757–5803

- Telephone the NASA STI Help Desk at 443–757–5802

- Write to:
  NASA Center for AeroSpace Information (CASI)
  7115 Standard Drive
  Hanover, MD 21076–1320

NASA/TM—2011-216946 AIAA–2010–7670

Experimental Observations on the Deformation and Breakup of Water Droplets Near the Leading Edge of an Airfoil

Mario Vargas
Glenn Research Center, Cleveland, Ohio

Alex Feo
Instituto Nacional de Técnica Aeroespacial, Madrid, Spain

Prepared for the
Atmospheric and Space Environments Conference
sponsored by the American Institute of Aeronautics and Astronautics
Toronto, Ontario, Canada, August 2–5, 2010

National Aeronautics and
Space Administration

Glenn Research Center
Cleveland, Ohio 44135

January 2011

Acknowledgments

The authors would like to thank Mr. Chris Lynch and Mr. Quentin Schwinn for their outstanding high speed imaging work during the experiment. Thanks also to Mr. Yago Sánchez and Mr. Carlos Molina from ALAVA INGENIEROS for their generosity in allowing us to use the Photron camera during the experiment and for their support and expertise during the experiment. Thanks Mr. Miguel Guerra-Valles for his help during the experiment and for establishing the procedure to align the camera with the airfoil. Thanks to all rotating rig INTA personnel for their excellent support in the preparation work and during the execution of the test program. Special thanks to Mr. Suthyuvann Sor for his excellent engineering support and for upgrading the rotating rig to its present state. Also thanks to Ms. Eva Jarillo for her dedication to the NASA/INTA cooperation and in the development and calibration of the Monodisperse droplet generator used during the test program. Thanks to Dr. Andy Broeren for his help with the monosize droplet generator during the pre-test imaging work done at the Icing Branch Flow Laboratory. The present work is part of the NASA/INTA collaboration under a Space Act Agreement. It is funded under the NASA Integrated Resilient Aircraft Controls (IRAC) Project of the Aviation Safety Program. The authors would like to thank Dr. OA Guo, Mr. Gene Addy and the Project Office for their support.

Level of Review: This material has been technically reviewed by technical management.

Available from

NASA Center for Aerospace Information
7115 Standard Drive
Hanover, MD 21076–1320

National Technical Information Service
5301 Shawnee Road
Alexandria, VA 22312

Available electronically at http://www.sti.nasa.gov

Experimental Observations on the Deformation and Breakup of Water Droplets Near the Leading Edge of an Airfoil

Mario Vargas
National Aeronautics and Space Administration
Glenn Research Center
Cleveland, Ohio 44135

Alex Feo
Instituto Nacional de Técnica Aeroespacial
Madrid, Spain

This work presents the results of an experimental study on droplet deformation and breakup near the leading edge of an airfoil. The experiment was conducted in the rotating rig test cell at the Instituto Nacional de Técnica Aeroespacial (INTA) in Madrid, Spain. An airfoil model placed at the end of the rotating arm was moved at speeds of 50 to 90 m/sec. A monosize droplet generator was employed to produce droplets that were allowed to fall from above, perpendicular to the path of the airfoil at a given location. High speed imaging was employed to observe the interaction between the droplets and the airfoil. The high speed imaging allowed observation of droplet deformation and breakup as the droplet approached the airfoil near the stagnation line. A tracking software program was used to measure from the high speed movies the horizontal and vertical displacement of the droplet against time. The velocity, acceleration, Weber number, Bond number, Reynolds number, and the drag coefficients were calculated along the path of a given droplet from beginning of deformation to breakup and/or hitting the airfoil. Results are presented for droplets with a diameter of 490 micrometers at airfoil speeds of 50, 60, 70, 80 and 90 m/sec.

Nomenclature

avi	=	Audio video interleave movie format
V	=	Velocity, mph
T_{total}	=	Total temperature, ^{o}F
LWC	=	Cloud liquid water content, g/m^3
MVD	=	Water droplet median volume diameter, μm
DBKUP 002	=	Designation for Airfoil used in the experiment
SLD	=	Supercooled Large Droplets
INTA	=	Instituto Nacional de Técnica Aeroespacial
ITC	=	Imaging Technology Center at NASA Glenn Research Center
LED	=	Light Emitting Diode
Slip Velocity	=	Relative velocity between the droplet and the air: ($\mathbf{V}_{droplet}$ - $\mathbf{V}_{air}$)
TSIT	=	Time-Sequence Imaging Technique

I. Introduction

Aircraft manufacturers have reported in-flight observation of droplet breakup near the wing surfaces of large transport aircraft[1]. This observation is important for in-flight icing because if large droplets break up before impinging on aircraft surfaces, the smaller droplets that result may not impinge on the airfoil potentially affecting the ice accretion process. If droplet breakup is a factor in the ice accretion process, current ice accretion codes will need to be modified to account for the breakup phenomena.

A large body of research exists on droplet deformation and breakup. Those studies are related to nozzle spray systems, fuel injection, liquid propellants, aerosol atomization, mixture formation in internal combustion engines, ink jet printing and spray drying among others. The experimental configurations used in those studies are completely different from droplets impinging on an airfoil. Only the configurations used by Wierzba[2], Kennedy and Roberts[3], Suzuki and Mitachi[4] have some similarities although no airfoil was used in those studies. Wierzba studied the critical Weber numbers (Weber number at the time of droplet breakup) when droplets are released normal to an instantaneous air flow in a horizontal wind tunnel. Kennedy and Roberts studied the breakup of droplets subject to an accelerating flow in a vertical wind tunnel. Droplets were released at the inlet of the tunnel and accelerated toward the test section of the tunnel where observations were conducted. In the process, a relative gas-droplet velocity was generated and was one of the parameters varied but they did not study the effect of the change of the relative velocity with time on the critical Weber number or the breakup time of the droplets. Susuki and Mitachi studied the effect of a linearly increasing relative droplet gas velocity on the droplet breakup. In their configuration the droplets were released into the unsteady droplet-gas velocity flow. They found that the critical Weber number increased as the rate of relative droplet-gas velocity was increased at the injection location. Although the experiments by Wierzba, Kennedy and Roberts, Suzuki and Mitachi included a relative droplet-gas velocity, only Suzuki and Mitachi studied the effect of varying the relative velocity with time. In no case was an airfoil used as an experimental configuration.

In 2005 the Federal Aviation Administration (FAA) sponsored a computational study by Wichita State University (Tan, Papadakis and Sampath[1]) to assess the effects of aerodynamic forces on water droplets near the leading edge of an airfoil and the leading edges of the slat and flap elements of a high-lift airfoil. Two-dimensional numerical computations of droplet breakup were done using the TAB model in the commercial code Fluent. The TAB model used included only vibrational and bag models of breakup. The effect of chord size and droplet diameter was studied for a NACA 0012 geometry for chords of 3 feet and 20 feet and droplet sizes of 100, 500 and 1000 micrometers. For the case of a 20-foot chord airfoil, droplet breakup was studied for a three element airfoil high lift system in a landing configuration. The study indicated that droplets may breakup in regions with severe pressure gradient. For the 3-foot chord single element airfoil the droplet breakup occurred aft of the leading edge. For the 20-foot chord single element airfoil the droplet breakup occurred near the stagnation region only. Large droplets were found to be more susceptible to breakup than smaller ones. They found that when droplet breakup occurred near the airfoil surface there was insufficient distance between the airfoil wall and the location where the droplet breakup was initiated for the droplets to achieve complete breakup before hitting the airfoil. The trajectory followed by droplets larger than 500 micrometers were “ballistic” in nature. The study pointed out the lack of experimental data in this area and recommended experimental tests to assess the effects on droplet breakup and breakup modes from the pressure gradient and the relative droplet-gas velocity near the leading edge of an airfoil.

In 2007 the National Aeronautics and Space Administration (NASA) and the Instituto Nacional de Técnica Aeroespacial (INTA) in Madrid, Spain, began an experimental research program to obtain droplet breakup data on an airfoil configuration. A droplet breakup rotating rig[5] was designed and built at the INTA installations near Madrid. The first sets of experiments were conducted at low speeds (15-66 m/s) in the fall of 2008. Using the experience gained from the low speed experiment the test rig was modified to attain speeds up to 90 m/sec.

The present work reports the results of a droplet deformation and breakup experiment conducted in the spring of 2010. The objective of the experiment was to use high speed imaging to observe the droplet deformation and breakup and to measure the important parameters as the droplet approaches an airfoil near the stagnation line. The experiment was conducted in the rotating rig test cell at the Instituto Nacional de Técnica Aeroespacial (INTA) in Madrid, Spain. An airfoil model placed at the end of the rotating arm was moved at speeds of 50 to 90 m/sec. A monosize droplet generator was employed to produce droplets from 100 to 500 micrometers that were allowed to fall from above perpendicular to the path of the model airfoil at a given location. High speed imaging was employed

to observe the interaction between the droplets and the airfoil, and droplet deformation and breakup. A tracking software program was used to measure from the high speed movies the droplet horizontal and vertical displacement against time. The horizontal displacement data was curve fitted to obtain the velocity and acceleration. The velocity and acceleration, together with experimental values of the air velocity at the locations of the droplet, were used to calculate the Weber number, Reynolds number, Bond number, and the drag coefficients along the path of the droplet from beginning of deformation to breakup and/or hitting the airfoil. Observations and measurements were conducted near the leading edge of an airfoil for velocities from 50 to 90 m/sec for a droplet size of 490 micrometers.

The present work is the first time that a systematic study of droplet deformation and breakup has been conducted for droplets approaching the leading edge of an airfoil and the first time that the important parameters and dimensionless numbers have been directly measured along the path of the droplets from initial deformation to breakup and/or hitting the airfoil. The results have provided critical information on how the droplet breakup occurs and experimental measurements of the critical parameters involved. The results have also provided a clear view of the next steps to be followed in the experimental program.

II. Experimental Setup

The experimental setup has four main elements: the rotating arm unit, the airfoil attached at the end of the arm, the monosize droplet generator and the high speed imaging system. Figure 1 shows the conceptual view of the experiment setup with all the elements except the high speed imaging system. Figure 2 shows the experimental setup components in the test cell before a run.

A. Rotating Arm Unit

The rotating arm unit consists of a 5 kW electric motor mounted on a support structure that rests on a solid base attached to the floor (Fig. 2). The support structure is attached to the base through four slip ring vibration dampers. The motor is placed inside the support structure with the axle perpendicular to the horizontal plane and in the direction of the ceiling. A rotating arm is attached to the axle of the motor. The length of the arm measured from the center of the axle to the airfoil model attached at the end is 2.37 meters (93.3 inches). For balancing, vibration control and additional strength, a system of struts is mounted on the axle and opposite the arm location (Fig. 2). Accelerometers on the arm and the axle are used to monitor the arm vibrations. The revolutions per minute of the arm are measured using a light emitting diode (LED) optical system. The LED is mounted on the supporting structure with its beam pointed at an angle toward the rotating axle. A small reflecting tape mounted on the rotating axle reflects the light in each revolution. The reflected light is picked up by a detector placed next to the LED. Each time that the detector registers the reflected light from the LED one revolution of the arm is counted. The control of the electric motor is located in the control room, a section of the test cell separated from the rotating rig by a safety glass window (Fig 2). The revolutions per minute of the arm can be adjusted to set the airfoil model at velocities from 0 to 90 m/sec at less than 1m/sec intervals.

B. Airfoil Model

The airfoil model mounted at the end of the rotating arm is a generic type of thick airfoil designated as DBKUP 002 (Fig. 3). Table I list the coordinates of the airfoil. The airfoil was chosen for the experiment because it has a blunt shape geometry that simulates a scaled version of the type of leading edge shape found on large transport airfoils. The airfoil measures 0.35 meters (13.78 inches) in the spanwise direction, and has a chord length of 0.47 meters (18.5 inches).

C. Monosize Droplet Generator

A TSI MDG-100 Monosize Droplet Generator is used to produce water droplets within a diameter range from 100 μm to 500 μm. The droplet generator (Fig. 4) consists of a water pressure container, a flow control valve, a frequency generator and the vibration head. Air from a compressor pressurizes the tank and generates the water flow from the tank to the vibration head. A high precision flow rate control valve with a manometer allows fine adjustment of the flow rate before the water flow reaches the vibration head. At the vibration head the water is forced through a small orifice (100 μm in diameter) and a jet is formed. A disturbance in the form of a square wave at the appropriate frequency is introduced by activating a piezoelectric transducer controlled with a BK Precision model 4011A frequency generator. The jet is unstable at resonant frequencies and breaks into uniform droplets. For

a given orifice diameter, flow rate and excitation frequency the diameter of the droplets generated is given by the equation:

$$D(\mu m) = 317\left[\frac{Q_{(cc/\min)}}{f_{(kHz)}}\right]^{1/3}$$

Where Q is the water flow rate in cubic centimeters per minute; f is the frequency in kilohertz; and D is the diameter of the droplets in micrometers. Previous to the droplet breakup high speed test, the monosize droplet generator was calibrated[6] against a Phase Doppler Particle Analyzer (PDPA) for orifices of 50 and 100 μm. During the experiment only the 100μm orifice was used.

D. High Speed Imaging System

The high speed imaging system consists of the high speed camera, the camera software, the lens system and the lightning (Fig. 5). The high speed camera used during the experiment was a Photron SA-5. The camera can capture images at rates from 1,000 to 1,000,000 frames per second (fps). During the experiment frames rates of 25,000, 50,000, 65,100, 75,000, 100,000 and 150,000 fps were used with corresponding resolutions given in pixels for the horizontal and vertical directions: 512x512, 192x512, 246x320, 192x312, 192x264 and 128x184. As the frame rate is increased the resolution of the camera decreases. The camera has a maximum shutter speed of 1microsecond (μs) at frames rates below 775,000 fps. The camera software employed for capturing the high speed image sequences is Photron's FASTCAM Viewer (PFV) and is part of the camera system. The same software was used for post-processing the image sequences to generate the data movies for data analysis. During the experiment one lens configuration was used for two magnifications of the droplet deformation and/or breakup. The lens configuration consisted of a 200mm Micro Nikkor lens with a 2x doubler added between the camera and the 200mm lens to double the focal length of the microlens. The two magnifications were achieved by placing the camera at two different distances from the location where the droplets were falling at 0.24 meters (9.25 inches) along the span of the airfoil. For the first magnification the distance was 0.91 meters (36 inches) and for the second the distance was 0.36 meters (14 inches). The lightning was designed to illuminate the droplets from behind to create a shadowgraph (black color of the droplets against a white-gray background). The light source was a 2000 watt Xenon light with a lens to focus the beam.

III. Test Procedure and Test Matrix

A. Test Procedure

Before a test run, the high speed camera system needs to be aligned, so that the line of view of the lens is parallel with the direction along the span of the airfoil at the midpoint of the leading edge (stagnation line along the span). The rotating arm is set at the position, where the falling droplets from the monosize droplet generator will just graze the leading edge. The airfoil is held at the same location during the whole alignment process. The camera is placed at the distance required by the optics to obtain the needed magnification and such that the center of the lens depth of field is at the location where the falling droplets graze the airfoil leading edge. A rectangular steel beam (extending from the airfoil to the camera) is placed parallel to the span the airfoil (grazing it) and parallel to the side of the camera. This ensures that the direction of the lens is parallel to the direction of the airfoil span but displaced a known distance. The steel beam is removed and the camera and lens are moved to a position where the lens direction is aligned, grazing the leading edge along the span of the airfoil. The motion of the camera can be carefully controlled because the camera sits on a x-y positioning table.

The airfoil is moved from the alignment position and a ruler with the smallest subdivision of one millimeter is placed at the location where the droplets will graze the leading edge of the airfoil. The camera is focus on the ruler and the number of pixels per millimeter is recorded, since the number of pixels in the camera sensor and the field of view are known. This conversion is used during the data analysis to measure the droplet diameter.

The monosize droplet generator controls are adjusted to produce the range of droplet sizes needed. The pressure and the frequency values are read from the calibration table obtained during the previous calibration of the system[6]

for the orifice being used in the generator (100 μm). Table 2 shows the calibration table used to setup the monosize droplet generator conditions. The pressure valve and the frequency generator are set at the corresponding values and the generator is started.

The personnel withdraw to the control room, where they are able to observe the motion and operation of the rotating arm through the safety glass. The camera is controlled with software run on a laptop computer located in the control room (Fig. 4.) The software is used to start the camera and set the controlling parameters including the frame rate and the shutter speed. The software allows writing information that will be part of the camera frames. It is located on each frame above the recorded image. This information is helpful during the data analysis. During the experiment the following information was recorded on each frame: frame rate, time of recording, image resolution, frame number, lens configuration, date and time, arm velocity and target droplet size.

The rotating arm is set in motion at the revolutions per minute (rpm) corresponding to the target velocity. When it reaches the target speed, the camera recording is started and maintained for three rotations. Once the recording is completed the rotating arm is brought to a stop. The high speed movie is analyzed with the camera software to determine the quality of the recording in each of the three passes of the airfoil. If the recording is deemed of good quality the experiment moves to the next test point and the process is repeated.

B. Test Matrix

Table 3 shows the test matrix for the experiment. The strategy followed was to setup the droplet generator for theoretical droplet diameters of 523, 415, 332, 191, 138 and 114 μm. At each droplet size test points were for airfoil velocities of 50, 60, 70, 80 and 90 meters per second. Frame rate values employed were: 25,000, 50,000, 65,100, 75,000, 87,000, 100,000 and 150,000 fps with 75,000 fps being the most used because it was a middle point between a frame rate that allowed observation of the droplet breakup and a reasonable resolution of 192x312 pixels. Table 3 shows the run number, the calibration point for the monosize droplet generator taken from Table 2, the theoretical droplet diameter, the airfoil velocity, the lens magnification, the camera resolution and the frame rate. Two camera magnifications were employed during the test. The larger magnification gave more detail but it only allows observation of the droplets over a very small distance. The smaller magnification allows to observe the droplet over a larger distance, from no interaction with the airfoil, to beginning of deformation, deformation and breakup or impact with the airfoil.

IV. Data Analysis

A. Tracking a Single Droplet to obtain the Droplet Displacement against Time

The data analysis is performed using the software program Spotlight-8[7] that allows frame by frame study of the movies, zooming in and out on single frames, running the movies forward and backward, and tracking a single droplet in x-y directions. Before each movie is analyzed with Spotlight 8 the camera software is used to convert from the camera format to audio video interleave (avi) format without any compression to avoid modifying the data.

Using Spotlight-8, a high speed movie corresponding to a set of experimental conditions is opened and the frames where the airfoil impacts the droplets are located. There are three of those frames per movie, because during the test, the camera is programmed to capture three rotations of the airfoil. In general several droplets can be observed impacting the airfoil and in some cases breaking up before impact. The movie is run backward and forward to study the behavior of the droplets before and during their interaction with the airfoil. A droplet is selected for study and the program is returned to the frame where the airfoil is about to hit the droplet. The droplet may be deforming or is in the process of breaking up. A copy of the frame is saved in the experimental notes and the droplet to be studied is labeled for future identification (Fig. 6). The movie is run backward to the frame where there is no indication of deformation or interaction of the droplet with the approaching airfoil and where the tracking is going to be initiated.

Before tracking the droplet, its diameter is measured at or near the frame where the tracking is going to be started. Zooming-in on the droplet, the number of pixels that form the droplet are counted in the horizontal and vertical directions and averaged (Fig. 7). The conversion of number of pixels to millimeters is used to obtain the diameter of the droplet in metric units. The counting of the number of pixels can introduce an error in the measurement of ±1 pixel in cases where it is difficult to determine the boundary of the droplet shape. In the case of

droplets with a diameter of 490 μm, for which the results are discussed in Section V, the error in the measurement could be as high as 14% depending on how well defined is the shape of the droplet on the image used to measure the diameter.

Tracking is initiated by zooming-in on the droplet and using the threshold option to create a white background against the black droplet image but adjusting the threshold to maintain the same droplet shape. The center of mass tracking capability in Spotlight-8 is selected and the droplet image is enclosed in a rectangle, or region of interest (Fig. 8). After zooming out to see the whole threshold image frame, the program tracks the motion of the droplet. After tracking on a given frame, the region of interest is repositioned on the centroid of the tracked object. The tracking is followed on the computer screen and terminated just after the airfoil strikes the droplet. The tracking data is saved as a text file with the centroid position of the droplet at each frame given in (x,y) coordinates with respect to the first tracking frame. In the output file the data is displayed in three columns: one for the x coordinate, one for the y coordinate and one for the frame number. At each row in the table, the (x,y) coordinate and the corresponding frame are listed. The data is then transferred to an Excel spreadsheet. In the Excel spreadsheet the x and y coordinates of the droplet are converted from pixels to metric units. Since the inverse of the camera frame rate gives the time separation between each frame, the time associated with each (x,y) displacement can be obtained after taking the first tracking frame as the starting time. The droplet displacement against time can be plotted (Figure 9). It is the droplet displacement measured by an observer located on a frame of reference at rest with respect to the control room in the test cell.

B. Effect of the Camera Resolution on the tracked Droplet Displacement against Time

To capture the behavior of the droplets and especially droplet breakup, it is necessary to go to frame rates higher than 50,000 fps because breakup occurs very close to the leading edge and in a reduced time frame window. The higher the frame rate the more frames will be captured in that reduced time frame where breakup occurs. The downside of higher frame rates is lower resolution. For a given frame rate the camera can sustain a given maximum resolution and the higher the resolution, the lower the frame rate. It is a limitation in the current technology of high speed cameras and it is related to the time that it takes for the camera system to extract the information from the sensor. Table 4 lists the resolutions for the frame rates used during the experiment. A frame rate of 75,000 was found to be the best compromise between frame rate and resolution and it was the frame rate most used as can be seen in the test matrix (Table 3). The combination of the optical configuration (lens, doubler, magnification), the high camera frame rate, the corresponding low resolution and the droplet moving at low speed affects the tracking data in the following way: at a high frame rate the time between frames is a few microseconds and during that time a droplet moving at low speed will cover a distance that is shorter than the physical dimension of a pixel in the camera sensor. The tracking data will indicate that the droplet remained at the same location when it is actually in motion. This can be seen in Figure 9. At the lower times the droplet seems to remain at the same location for a period of time. As the droplet speed increases the effect decreases and the droplet appears to remain at the same location less and less.

As an example, for a camera frame rate of 75,000 fps the maximum resolution possible is 192x312 pixels. At this resolution, for the optical configuration used, a scale on the field of view indicates that there are 14.295 pixels per millimeter in the horizontal direction; therefore each pixel is 70 μm wide. At a frame rate of 75,000 fps each frame is separated by 13.33 μsec. A droplet moving across the field of view at a velocity of less than 70μm/13.33μsec (5.24 meter per second) won't transverse a pixel in 13.33 μsec and will be tracked as remaining in the same location. If the droplet were moving at 1 meter per second (equivalent to 1μm/μsec), it would take the droplet 70μsec to cover a distance equivalent to the width of a pixel and it would be recorded by the tracking program as remaining in the same location for 70μsec/13.333μsec or 5 camera frames.

C. Calculation of the Horizontal Velocity and Acceleration of the Droplet against Time

The horizontal velocity and acceleration of the droplet are calculated from the curve fit of the droplet displacement against time. The data points in the plot are curve-fit with a double five parameter exponential growth equation (Fig. 9). The first and second derivatives of the curve-fit equation give the droplet velocity and acceleration (Fig. 10 and Fig. 11). Those are the droplet horizontal velocity and acceleration against time measured by an observer located on a frame of reference at rest with respect to the test cell.

D. Change from the Frame of Reference at the Test Cell to the Frame of Reference at the Airfoil

The horizontal displacement, velocity and acceleration were initially measured in a frame of reference at rest with respect to the test cell. It is more convenient to work in a frame of reference at rest on the airfoil. The frame of reference located on the airfoil is shown in Figure 12. The origin is located at the stagnation point on the leading edge. In a strict sense, a frame of coordinates at rest with respect to the airfoil is not an inertial frame because the airfoil is rotating, it is accelerated. Since the interaction between the droplets and the airfoil occurs at a distance less than or equal to the airfoil chord, that section of the airfoil path is nearly straight and the frame of reference at rest with respect to the airfoil is assumed as inertial during that part of its path. The Galilean transformation together with the airfoil velocity was used to convert the velocity and acceleration of the droplet from the frame of reference at the test cell to the frame of reference at the airfoil (Fig.13 and Fig. 14).

E. Position of a Droplet with respect to the Frame of Reference at the Airfoil

At a given location along the droplet path, the number of camera frames separating the droplet from the airfoil is equal to the frame number at which the airfoil hits the droplet minus the frame number at the given location of the droplet. Multiplying the number of frames separating the droplet and the airfoil by the time lapse between frames (1/frame rate) and by the airfoil speed gives the horizontal position of the droplet with respect to the frame of reference at the airfoil. Repeating the calculation for each droplet location gives the distance of the droplet along its horizontal path with respect to the leading edge of the airfoil. The main parameters in the experiment were calculated at each position of the droplet as it approaches the airfoil and with respect to the frame of reference located at rest on the airfoil.

F. Air Velocity at a given Droplet Location

For an airfoil with the same geometry as the DBKUP 0012 but scaled down 1/10 in size (0.047m chord), the air velocity along the horizontal line ending at the stagnation point on the leading edge was measured experimentally with a Laser Droplet Velocimeter (LDV) at the INTA 0.3mx0.2m wind tunnel. Figure 15 shows the results. The vertical axis in the plot records the air velocity divided by the free stream velocity (V_{air}/V_{α}). The horizontal axis records the distance with respect to the leading edge of the airfoil divided by the chord (x/c). The experimental data was curve-fit (Fig. 15) and the resulting equation was used to calculate the air velocity at any given droplet position along its path. To calculate the position of the droplet using the curve-fit equation the value of the free stream velocity is needed. For the frame of reference at rest with respect to the airfoil, the air free stream velocity is the same as the velocity of the airfoil with respect to the frame of reference at rest with respect to the test cell.

G. Relative Velocity between the Droplet and the Air (Slip Velocity)

Since at each droplet position along its path the horizontal velocity of the droplet and the velocity of the air are known, the relative velocity between the droplet and the air can be calculated. This velocity, V_{air}-$V_{droplet}$, is called the "slip velocity". The Reynolds number, the Weber number and the drag coefficient can be calculated when the horizontal slip velocity at each location along the droplet path is known

H. Calculation of the Reynolds Number, the Weber Number, the Bond Number and the Drag Coefficient

The main parameters measured along the path of the droplet were the Reynolds number, the Weber number, the Bond Number and the Drag coefficient. All those parameters were measured with respect to the horizontal motion of the droplet. The droplets leave the monosize droplet generator and fall vertically at a constant speed between 7-10 m/sec (measured during the experiment). There was no indication from the physical behavior of the droplet that the vertical velocity had an influence on the deformation of the droplet. The shape of the droplet during deformation corresponded to the response of the droplet to the horizontal velocity and acceleration. In all the measurements and calculations the vertical velocity was not considered.

The following are the definitions of the main parameters measured along the path of the droplet:

Reynolds Number $$\mathrm{Re} = \frac{\rho_{air}\left|V_{air} - V_{droplet}\right| D}{\mu_{air}}$$

Weber Number $$We = \frac{\rho_{air}\left|V_{air} - V_{droplet}\right|^2 D}{\sigma_{water\,/\,air}}$$

Bond Number $$Bo = \frac{\rho_{water} D^2}{\sigma_{water/air}} \left(\frac{dV_{droplet}}{dt} \right)$$

Drag Coefficient $$Cd = \frac{4}{3} \frac{\rho_{water}}{\rho_{air}} \frac{D}{\left| V_{air} - V_{droplet} \right|^2} \frac{dV_{droplet}}{dt}$$

where D is the droplet diameter, $V_{droplet}$ is the droplet velocity, V_{air} is the air velocity at the location of the droplet, $(V_{air} - V_{droplet})$ is the slip velocity, ρ_{air} is the air density, μ_{air} is the air absolute viscosity, ρ_{water} is the water density for the droplet, $\sigma_{water/air}$ is the water surface tension for the droplet. The Bond number was defined with respect to the droplet acceleration.

Since the air and water droplet properties are known and the droplet diameter, the slip velocity and the droplet acceleration are measured or calculated along the path of the droplet, then the non-dimensional parameters can be calculated. The velocities and accelerations employed in the calculation of the parameters are for the horizontal direction.

Figures 16, 17, 18 and 19 show the Reynolds number, the Weber number, the Bond number and the drag coefficient for the case of a droplet with a diameter of 490 μm, when the airfoil speed is 90 m/sec, the camera frame rate 75,000 fps and the resolution 192x312 pixels. The horizontal displacement and acceleration presented in Figures 9,10,11,13 and 14 are for the same droplet.

I. Forces acting on a Droplet as it approaches the Airfoil

A brief comment is needed on the forces acting on a droplet approaching the airfoil. The forces acting on a droplet in a non-uniform flow field[8] ignoring particle rotation, slip in the shear flow of a boundary layer and other effects are: the pressure gradient force, the virtual mass force, the viscous drag force, the Basset force and the force of gravity. When $\rho_{droplet}$ is about three orders of magnitude or greater than ρ_{air} (999.7 kg/m^3 vs. 1.205 kg/m^3) only the viscous drag force needs to be considered[8,9,10,11]. This approximation was tested on a limited number of droplets by calculating the pressure gradient force, the virtual mass force, the viscous drag force and the Basset force. To calculate the viscous drag force, the drag coefficient is needed and in the case of the water droplet it changes along the path of the droplet (Fig. 19) because the droplet is deforming, in a decelerating process. To calculate the viscous drag force the droplet was assumed to be spherical and the classical curve of drag coefficient versus Reynolds number was used. Since the Reynolds number for the droplets was measured between 900 and 3000, the drag coefficient in that part of the curve could be approximated by 0.46[12]. Using this value gives a lower bound value for the Viscous Drag Force, since the drag coefficient for deforming droplets tends to larger values than for the spherical droplet case. In all the cases the lower bound value of the viscous drag force was an order of magnitude larger than the other forces confirming the validity of the approximation. In the measurement of the drag coefficients at each location of the droplet as it approaches the airfoil the approximation was used and the drag coefficient was obtained from the equation:

$$\frac{\pi d^3_{droplet}}{6} \rho_{droplet} \frac{d\vec{V}_{droplet}}{dt} \approx \frac{\pi d^3_{droplet}}{8} \rho_{air} \frac{C_d}{d_{droplet}} \left| \vec{V}_{air} - \vec{V}_{droplet} \right| \left(\vec{V}_{air} - \vec{V}_{droplet} \right)$$

V. Results

At each velocity tested, the high speed movies were studied to determine the behavior of the droplets as they approached the airfoil. The frame by frame and zooming capability of the Spotlight 8 program allowed careful observation of how the droplets deform and in some case breakup. After those general observations were recorded, droplets with a 490 μm were selected at each airfoil velocity for tracking and calculation of the parameters. The parameters were calculated and compared to study the effect of the actual parameter and also the effect of velocity. The tracking and calculation of the parameters was done following the procedure described in the Data Analysis section IV.

A. Droplet Deformation as it approaches the Airfoil

Initially the droplets leave the monosize droplet generator and fall under the action of gravity at measured speeds between 7-10 m/sec (Fig 20). The largest droplets show oscillations as they fall. As the droplet gets closer to the airfoil its shape begins to distort and becomes flattened at the front side (the side closest to the airfoil) and bulging at the rear (Fig. 21). As the droplet gets closer and closer to the airfoil, the distortion changes and the droplet shape is thinner in the horizontal direction, more elongated in the vertical direction (Fig 21) and then begins showing a small bump in the middle on the side that is closest to the airfoil. The bump signals the beginning of a Bag-type breakup mechanism observed by previous studies in different configurations[2,13]. The initial formation and growth of the bag is the last stage observed before breakup (Fig 21and Fig 22). The smaller droplets generated with the monosize droplet generator were in the range of 100μm and the largest ones in the order of 560 μm. The smallest droplet showed the initial spheroid shape deformation only. The largest droplet showed all the deformation steps described above and in some cases they broke up. Figure 21 shows the typical sequence of deformation observed. The figure shows the droplet shape as it approaches the airfoil. Shown below each frame is the corresponding time, Weber Number and distance from the leading edge of the airfoil. Figure 22 shows the last stages of deformation; from the beginning of formation of the Bag mechanism of breakup to the actual breakup. The figure shows five frames each separated by 71.4 μsec. The original data movie had 15 frames each separated by 14.28 μsec and it lasted a total of 214 μsec from initial formation of the bag type breakup to the breakup.

All the observed droplet breakups occurred just before the droplet hit the airfoil. The breakup was observed to occur on some of the bigger droplets but not on all of them. The smaller droplets showed the initial stages of deformation but not breakup. For velocities of 50 m/sec and 60 m/sec no droplet breakup was observed. A limited number of droplets were observed to breakup at 70 m/sec. Nearly all the droplet breakups were observed at 80 and 90 m/sec.

B. Droplet Velocity and Acceleration as the Droplet approaches the Airfoil

In all the tracked droplets, the velocity and acceleration follows the same pattern: the velocity of the droplet decreases exponentially (Fig. 13) as the acceleration acting in the opposite direction of the droplet motion (deceleration) increases (Fig. 14). As the droplet velocity decreases the air velocity also decreases (Fig. 15) but at a higher rate. A relative velocity between the droplet and the air (slip velocity) develops and increases as the droplet approaches the airfoil, reaching a maximum when the droplet is about to hit the airfoil (Fig. 23). The case presented in figures 13-15 and 23 are for a droplet of 490 μm in diameter.

Although the droplet velocity decreases, the change in the velocity is not large with respect to the initial velocity of the droplet, but it occurs in a very short time and the acceleration acting on the droplet is very large. In the case of the droplet measurements shown in Figures 10, 11, 13 and 14 for a droplet of 490 μm, the velocity of the droplet decreases from 89 m/sec to 75 m/sec in 440 μsec or an average deceleration of 31,818 m/sec^2. The last deceleration calculated before the droplet impacts the airfoil was 118,034 m/sec^2.

C. Weber Number as the Droplet approaches the Airfoil

The Weber number represents the ratio of the inertial forces to the surface tension forces. Applied to a droplet approaching the airfoil, it compares the magnitude of the forces trying to pull the droplet apart to the surface tension force trying to keep the drop together. The Weber number is proportional to the square of the slip velocity. As the droplet approaches the airfoil the slip velocity develops and increases therefore the Weber number also increases (Fig. 17). Physically, it means that the inertia forces that pull apart the droplet are growing larger than the surface tension forces that keep the droplet together. As the inertial forces grow larger than the surface tension forces, the droplet is distorted and in cases where the inertial forces overwhelm the surface tension forces, breakup occurs. In

all the cases where the droplet breaks up the value of the calculated Weber number was between 30 and 50. The observed mechanism of breakup was the Bag type in all cases.

D. Reynolds and Bond Numbers as the Droplet approaches the Airfoil

As the droplet approaches the airfoil, the Reynolds number increases (Fig 16) because it is proportional to the slip velocity and the slip velocity increases as the droplet approaches the airfoil. For all the droplets tracked, the calculated Reynolds number was in the range between 200 and 3000. In all cases where the Bond number was calculated it increased as the droplet approached the airfoil (Fig. 18) because the absolute value of the droplet acceleration was increasing. Bond numbers as high as 389 were calculated prior to the droplet hitting the airfoil or breaking up.

E. Viscous Drag Force and Drag Coefficient as the Droplet approaches the Airfoil

For velocities of 80 and 90 m/sec and droplets of 490 μm diameter, as the droplet approaches the airfoil the drag coefficient increases (Fig. 19). The higher value calculated occurred just before the droplet breaks up or impinges on the airfoil. Those values can be compared to the case of a disk. For a circular disk the expected value of the drag coefficient is 3.6 times higher than the one expected for the classical case of the spherical droplet in a uniform flow field. Since the Reynolds numbers measured for the droplets fell between 900 and 3000, the value for the spherical droplet in that range can be approximated to 0.46 therefore the expected value for a disk is 1.7 in a uniform flow. In all case, the higher values of the drag coefficient were larger than the values expected for a disk. The reason may be that although the droplet in the last stages of deformation resembles a disk shape, the droplet is not a solid body and it is deforming and being decelerated. At a velocity of 70 m/sec the drag coefficient initially increases and then slightly decreases. At velocities of 50 and 60 m/sec the drag coefficient decreases as the droplet approaches the airfoil. These results should not be taken as general statements because measurements on other droplets indicate that the drag coefficient tendency may be different for different droplets. The actual deformation of an individual droplet as it approaches the leading edge of the airfoil influences the drag coefficient.

F. Airfoil Velocity Effect for Droplets of 490μm Diameter

At each airfoil velocity of 50, 60, 70, 80 and 90 m/sec, a droplet of 490μm diameter was selected for tracking and the Weber number was measured and compared. Figure 24 shows the Weber number against the distance from the leading edge of the airfoil. This is the Weber number measured in a frame of reference at rest with respect to the airfoil. At a given airfoil velocity (initial droplet velocity with respect to the frame of reference on the airfoil), the Weber number increases as the droplet approaches the airfoil leading edge, and the higher the velocity the larger the value of the Weber number. This should be expected since the higher the airfoil velocity, the larger the slip velocity that the droplet can experience and the larger the Weber number that the drop can reach. For velocities of 70, 80 and 90 m/sec the droplet breaks up before hitting the airfoil. For the droplets at 50 and 60m/sec the droplet did not breakup before hitting the airfoil.

In general, at a Weber number of 10 the droplets show the change of shape that indicates the beginning of deformation. In Figure 24 a horizontal line at a Weber number of 10 can considered as the boundary above where the droplets are beginning deformation for a given velocity. The graph shows that as the velocity increases, the deformation begins further away from the leading edge of the airfoil. For the droplets in Figure 24, the time that the droplet remains at a Weber number greater than 10 was calculated. It showed that the higher the airfoil velocity the longer the droplet remains at a Weber number larger than 10. The times for the airfoil velocities of 90, 80, 70, 60 and 50 m/sec were 587, 547, 480, 280 and 160 μsec respectively. At a higher airfoil velocity (higher initial droplet velocity in the frame of reference at rest with respect to the airfoil), the droplet experiences higher Weber numbers for longer times.

Figures 25, 26, 27, 28 and 29 show the effect of the airfoil velocity on the droplet velocity, acceleration, slip velocity, Reynolds number and Bond number.

VI. Conclusions

Experimental observation, measurement and calculation of the main parameters for droplets impinging on the leading edge of a DBKUP 002 airfoil was conducted with a specially designed rotating rig. The airfoil was mounted at the end of the rotating arm and water droplets from a monosize droplet generator were allowed to fall vertically at

a location on the airfoil path. The deformation and breakup of the droplets was captured using high speed imaging. The data movies were analyzed using a software package to determine the behavior of the droplets as they approached the airfoil and to measure the droplet horizontal and vertical displacement against time, and to calculate the velocity, acceleration, slip velocity, Weber number, Reynolds number, Bond number and drag coefficient at each point along the horizontal location of the droplet as it approached the leading edge of the airfoil. Measurements were conducted at five airfoil velocities: 50, 60, 70, 80 and 90 m/sec for droplets of 490 μm and the effect of the velocity were studied.

The following are the main conclusions from the observation and measurements:

- As droplets approach the airfoil they change shape and deform following a well defined pattern: the droplet falling under the action of gravity shows oscillations; as it approaches the airfoil it begins distorting in the horizontal direction by becoming flattened at the front (the side nearest the airfoil) and bulging at the rear; the distortion continues with the shape changing to elongated in the vertical direction and thin in the horizontal direction; as the droplet gets very close to the airfoil the elongated shape begins to show a bump ("bag") in the middle of the front side and for some of the large droplets the bump or "bag" grows until the droplet breaks up.

- The pattern of deformation of the droplets and breakup follows the Bag type observed and reported by other researchers in past studies with other experimental configurations and disturbance types.

- All the observed droplet breakups occurred just before the droplet hit the airfoil.

- The breakup was observed to occur on some of the bigger droplets but not all of them. The smaller droplets show the initial stages of deformation but not breakup.

- For velocities of 50 m/sec and 60 m/sec no droplet breakup was observed. A limited number of droplets were observed to breakup at 70 m/sec. Nearly all the droplet breakups were observed at 80 and 90 m/sec.

- Measurements showed that as the droplet approaches the airfoil, the velocity decreases exponentially and the droplet is decelerated. The difference between the droplet velocity and the air velocity at each location along the droplet horizontal path creates a slip velocity that also increases exponentially as the droplet approaches the leading edge of the airfoil. The viscous drag force is proportional to the square of the slip velocity and as the slip velocity develops and increases, the force will also increase and begin deforming the droplet.

- Measurements indicated that the droplet deceleration increases exponentially as the droplet approaches the leading edge of the airfoil. The deceleration is very high because the decrease in velocity of the droplet occurs during a very short time.

- Values of the Weber number and Bond number along the path of the droplet increase as the droplet approaches the airfoil.

- Measurements on droplets of 490μm in diameter at each airfoil velocity of 50, 60, 70, 80 and 90 m/sec showed that at a higher airfoil velocity (higher initial droplet velocity in the frame of reference at rest with respect to the airfoil), the droplet experiences higher Weber numbers for longer times along its path which translates to higher inertia forces for longer times trying to pull the droplet apart against the surface tension force keeping the droplet together.

- For droplets of 490 μm diameter and velocities of 90 and 80 m/sec the drag coefficient increases as the droplet approaches the airfoil. For a velocity of 70 m/sec the drag coefficient slightly increases. For velocities of 60 and 50 m/sec the drag coefficient slightly decreases. These trends of the drag coefficient cannot be generalized. Additional measurements of the drag coefficient in other droplets indicate that its tendency may be different for different droplets. The actual deformation of an individual droplet influences the drag coefficient as the droplet approaches the airfoil.

The experimental results presented in this paper are the first time that droplet deformation and breakup are studied and measured for droplets impinging on the leading edge of an airfoil. No previous experimental observations and measurements existed in this configuration.

VII. Future Work

Much progress has been achieved in understanding and measuring droplet deformation and breakup since the program was started in 2007 but additional work is needed to expand the current research results. Additional experimental work is needed in the following areas:

1) Observation and measurement of droplet deformation and breakup on two geometrical scaled versions of the DBKUP 002 airfoil. One model scaled down to ½ size of the DBKUP 002 and another scaled up 2 times the size. This additional research will allow us to learn how to scale the droplet deformation, breakup and measurements to larger transport airfoils.
2) Repeat the experimental observations and measurements on two airfoils of the same size but different geometry than the DBKUP 002. These experiments will allow to determine the effect of airfoil geometry on the droplet deformation and breakup

References

[1] Tan, J., Papadakis, M., and Sampaht, M. K., "Computational Study of Large Droplet Breakup in the Vicinity of an Airfoil", DOT/FAA/AR-05/42, Final Report, October 2005.

[2] Wierzba, A., "Deformation and Breakup of Liquid Drops in a Gas Stream at Nearly Critical Weber Numbers," *Experiments in Fluid*s 9, 1990, pp. 59-64.

[3] Kennedy, J.B. and Roberts, J., "Rain Ingestion in a Gas Turbine Engine", *ILASS-Americas, Inst. of Liquid Atomization and Spray Systems, 4th Annual Conference, Hartford, CT, USA, 1990, pp. 154-186.*

[4] Suzuki T. and Mitachi, K., "Experimental Study on Aerodynamic Breakup of Liquid Droplets in Time-Dependent Relative Velocity Fields", *8th Int. Conf. Liquid Atomization and Spray Systems*, Pasadena, CA, July 2000.

[5] Feo, Alex., Vargas, M., and Sor, S., "Rotating Rig Development for Droplet Deformation/Breakup and Impact Experiments Induced by Aerodynamic Surfaces", to be published in 2011.

[6] Jarillo, E. and Feo, A., "Estudio Mediante Técnica Láser PDPA de la Formación de Gotas en el Generador de Gotas Monodisperso Aerometrics MDG-100", Instituto Nacional de Técnica Aeoroespacial (INTA) Document No. AE/TNO/4420/119/INTA/06, March 2006.

[7] Spotlight-8, Version 2005.09.12 by Robert B. Klimek and Ted W. Wright

[8] Rudinger, G.,"Flow of Solid Particle in Gases", *AGARD –AG-222*, 1976

[9] Hinze, J. O., "Turbulence", McGraw-Hill, New York, 1959

[10] Fuch, N. A.., " The Mechanics of Aerosols", McMillan, New York, 1964

[11]Hjelmfelt, A. T.and Mockros, L. F., "Motion of Discrete Particles in a Turbulent Fluid", *Appl. Sciences Res.,Vol. 16, pp. 149-161*, 1966

[12]Sabersky R. H., Acosta, A. J., and Hauptmann, E. G., "Fluid Flow", *2nd Edition, McMillan Publishing Co.*, 1971

[13] Arcoumanis, C., Gavaises M.,French B.,"Effect of Fuel Injection Process on the Structure of Diesel Sprays," *SAE paper 970799*, 1997

Table 1. DBKUP 002 Airfoil Coordinates

X-Coordinate	Y-Coordinate	X-Coordinate	Y-Coordinate
1.0000	0.0000	0.0000	0.0000
0.9989	-0.0009	0.0011	0.0139
0.9957	-0.0014	0.0043	0.0310
0.9904	-0.0025	0.0096	0.0498
0.9830	-0.0042	0.0170	0.0674
0.9735	-0.0064	0.0265	0.0842
0.9619	-0.0089	0.0381	0.1007
0.9484	-0.0120	0.0516	0.1170
0.9330	-0.0155	0.0670	0.1318
0.9157	-0.0195	0.0843	0.1458
0.8967	-0.0240	0.1033	0.1584
0.8759	-0.0291	0.1241	0.1700
0.8536	-0.0347	0.1465	0.1797
0.8297	-0.0410	0.1703	0.1880
0.8044	-0.0479	0.1956	0.1943
0.7778	-0.0554	0.2222	0.1985
0.7500	-0.0634	0.2500	0.2007
0.7211	-0.0721	0.2789	0.2006
0.6913	-0.0815	0.3087	0.1985
0.6607	-0.0915	0.3393	0.1938
0.6294	-0.1019	0.3706	0.1870
0.5976	-0.1128	0.4025	0.1780
0.5653	-0.1240	0.4347	0.1683
0.5327	-0.1353	0.4673	0.1577
0.5000	-0.1466	0.5000	0.1466
0.4673	-0.1577	0.5327	0.1353
0.4347	-0.1683	0.5653	0.1240
0.4025	-0.1780	0.5976	0.1128
0.3706	-0.1870	0.6294	0.1019
0.3393	-0.1938	0.6607	0.0915
0.3087	-0.1985	0.6913	0.0815
0.2789	-0.2006	0.7211	0.0721
0.2500	-0.2007	0.7500	0.0634
0.2222	-0.1985	0.7778	0.0554
0.1956	-0.1943	0.8044	0.0479
0.1703	-0.1880	0.8297	0.0410
0.1465	-0.1797	0.8536	0.0347
0.1241	-0.1700	0.8759	0.0291
0.1033	-0.1584	0.8967	0.0240
0.0843	-0.1458	0.9157	0.0195
0.0670	-0.1318	0.9330	0.0155
0.0516	-0.1170	0.9484	0.0120
0.0381	-0.1007	0.9619	0.0089
0.0265	-0.0842	0.9735	0.0064
0.0170	-0.0674	0.9830	0.0042
0.0096	-0.0498	0.9904	0.0025
0.0043	-0.0310	0.9957	0.0014
0.0011	-0.0139	0.9989	0.0009
0.0000	0.0000	1.0000	0.0000

Table 2. Calibration for Generation of Monosize Droplet Generator Conditions

						Monosize Droplet Generator theoretical	
Calibration Point	**Orifice μm**	**Pressure bar**	**Frequency kHz**	**Discharge Q ml/h**	**Discharge Q cc/min**	**Droplet Diameter μm**	**Droplet V_{exit} m/sec**
Punto 1	50	0.7	4.15	78	1.3	215.29	11.03
Punto 2	100	0.4	10.37	138	2.3	191.89	4.88
Punto 3	50	1.0	20.00	90	1.5	133.68	12.73
Punto 4	100	0.7	2.00	270	4.5	415.39	9.55
Punto 5	100	0.7	3.90	270	4.5	332.49	9.55
Punto 6	50	1.0	40.00	90	1.5	106.11	12.73
Punto 7	50	1.0	100.00	90	1.5	78.18	12.73
Punto 8	50	1.0	50.00	90	1.5	98.50	12.73
Punto 9	50	1.0	60.00	90	1.5	92.69	12.73
Punto 10	50	1.0	70.00	90	1.5	88.05	12.73
Punto 11	100	0.7	1.00	270	4.5	523.36	9.55
Punto 12	50	1.0	4.00	90	1.5	228.60	12.73
Punto 13	50	1.0	1.00	90	1.5	362.87	12.73
Punto 14	50	1.0	80.00	90	1.5	84.22	12.73
Punto 15 F Rayleigh	50	1.0	56.60	90	1.5	94.51	12.73
Punto 17	50	0.7	10.00	66	1.1	151.89	9.34
Punto 18	50	0.8	2.00	72	1.2	267.37	10.19
Punto 19	50	0.8	30.00	72	1.2	108.41	10.19
Punto 20	50	0.9	5.00	78	1.3	202.33	11.03
Punto 21	50	0.9	100.00	78	1.3	74.54	11.03
Punto 22	100	0.6	15.00	246	4.1	205.73	8.70
Punto 23	100	0.6	50.00	246	4.1	137.72	8.70
Punto 24 F Rayleigh	100	0.7	20.70	270	4.5	190.61	9.55
Punto 25	100	0.8	70.00	282	4.7	128.84	9.97
Punto 26	100	0.8	100.00	282	4.7	114.40	9.97

Table 3. Test Matrix

Run Number	Point from Calibration Table 1	Orifice μm	Droplet Theoretical Diameter μm	Airfoil Model Velocity m/sec	Magnification	Resolution H x V pixels	Frame Rate Frames/sec
012510.01	Punto 23	100	137.72	90	1	512 x 512	25,000
012510.02	Punto 23	100	137.72	90	1	192 x 512	50,000
012510.03	Punto 23	100	137.72	90	1	192 x 312	75,000
012510.04	Punto 23	100	137.72	90	1	192 x 264	100,000
012510.05	Punto 23	100	137.72	90	1	128 x 184	150,000
012510.06	Punto 23	100	137.72	80	1	192 x 312	75,000
012510.07	Punto 23	100	137.72	70	1	192 x 312	75,000
012510.08	Punto 23	100	137.72	60	1	192 x 312	75,000
012510.09	Punto 23	100	137.72	50	1	192 x 312	75,000
012510.10	Punto 24	100	190.61	90	1	192 x 312	75,000
012510.11	Punto 24	100	190.61	90	1	192 x 264	100,000
012510.12	Punto 24	100	190.61	90	1	128 x 184	150,000
012510.13	Punto 24	100	190.61	90	1	128 x 184	150,000
012510.14	Punto 24	100	190.61	90	1	128 x 184	150,000
012510.15	Punto 24	100	190.61	80	1	192 x 312	75,000
012510.16	Punto 24	100	190.61	70	1	192 x 312	75,000
012510.17	Punto 24	100	190.61	60	1	192 x 312	75,000
012510.18	Punto 24	100	190.61	50	1	192 x 312	75,000
012510.19	Punto 11	100	523.36	90	1	192 x 312	75,000
012510.20	Punto 11	100	523.36	90	1	192 x 312	75,000
012610.01	Punto 11	100	523.36	90	1	192 x 312	75,000
012610.02	Punto 11	100	523.36	90	1	192 x 312	87,500
012610.03	Punto 11	100	523.36	90	1	128 x 184	150,000
012610.04	Punto 11	100	523.36	90	1	128 x 184	150,000
012610.05	Punto 11	100	523.36	80	1	128 x 184	150,000
012610.06	Punto 11	100	523.36	70	1	192 x 312	75,000
012610.07	Punto 11	100	523.36	70	1	128 x 184	150,000
012610.08	Punto 11	100	523.36	60	1	192 x 312	75,000
012610.09	Punto 11	100	523.36	60	1	128 x 184	150,000
012610.10	Punto 11	100	523.36	50	1	192 x 312	75,000
012610.11	Punto 11	100	523.36	50	1	128 x 184	150,000

Table 3. Test Matrix (Continuation)

Run Number	Point from Calibration Table 1	Orifice μm	Droplet Theoretical Diameter μm	Airfoil Model Velocity m/sec	Magnification	Resolution H x V pixels	Frame Rate Frames/sec
012710.01	Punto 4	100	415.39	90	1	192 x 312	75,000
012710.02	Punto 4	100	415.39	80	1	192 x 312	75,000
012710.03	Punto 4	100	415.39	70	1	192 x 312	75,000
012710.04	Punto 4	100	415.39	60	1	192 x 312	75,000
012710.05	Punto 4	100	415.39	50	1	192 x 312	75,000
012710.06	Punto 4	100	415.39	90	1	192 x 312	75,000
012710.07	Punto 4	100	415.39	80	1	192 x 312	75,000
012710.08	Punto 4	100	415.39	70	1	192 x 312	75,000
012710.09	Punto 4	100	415.39	60	1	192 x 312	75,000
012710.10	Punto 4	100	415.39	50	1	192 x 312	75,000
012710.11	Punto 4	100	415.39	90	1	128 x 184	150,000
012710.12	Punto 4	100	415.39	80	1	128 x 184	150,000
012710.13	Punto 4	100	415.39	70	1	128 x 184	150,000
012710.14	Punto 4	100	415.39	60	1	128 x 184	150,000
012710.15	Punto 4	100	415.39	50	1	128 x 184	150,000
012710.16	Punto 5	100	332.49	90	1	192 x 312	75,000
012710.17	Punto 5	100	332.49	80	1	192 x 312	75,000
012710.18	Punto 5	100	332.49	70	1	192 x 312	75,000
012710.19	Punto 5	100	332.49	60	1	192 x 312	75,000
012710.20	Punto 5	100	332.49	50	1	192 x 312	75,000
012810.01	Punto 5	100	332.49	90	1	128 x 184	150,000
012810.02	Punto 5	100	332.49	90	1	128 x 184	150,000
012810.03	Punto 5	100	332.49	80	1	128 x 184	150,000
012810.04	Punto 5	100	332.49	70	1	128 x 184	150,000
012810.05	Punto 5	100	332.49	60	1	128 x 184	150,000
012810.06	Punto 5	100	332.49	50	1	128 x 184	150,000
012810.07	Punto 5	100	332.49	66	1	256 x 320	65,100
012810.07D	Punto 5	100	332.49	66	1	256 x 320	65,100
012810.08	Punto 11	100	523.36	90	1	192 x 400	70,000
012810.09	Punto 11	100	523.36	90	1	192 x 400	70,000
012810.10	Punto 11	100	523.36	90	1	192 x 400	70,000

Table 3. Test Matrix (Continuation)

Run Number	Point from Calibration Table 1	Orifice μm	Droplet Theoretical Diameter μm	Airfoil Model Velocity m/sec	Magnification	Resolution H x V pixels	Frame Rate Frames/sec
012910.01	Punto 11	100	523.36	0	2	256 x 320	65,100
012910.02	Punto 4	100	415.39	0	2	256 x 320	65,100
012910.03	Punto 5	100	332.49	0	2	256 x 320	65,100
012910.04	Punto 24	100	190.61	0	2	256 x 320	65,100
012910.05	Punto 23	100	137.72	0	2	256 x 320	65,100
012910.06	Punto 26	100	114.4	0	2	256 x 320	65,100
012910.07	Punto 11	100	523.36	90	2	192 x 400	70,000
012910.08	Punto 11	100	523.36	90	2	192 x 400	70,000
012910.09	Punto 11	100	523.36	80	2	192 x 400	70,000
012910.10	Punto 11	100	523.36	70	2	192 x 400	70,000
012910.11	Punto 4	100	415.39	90	2	192 x 400	70,000
012910.12	Punto 4	100	415.39	80	2	192 x 400	70,000
012910.13	Punto 5	100	332.49	80	2	192 x 400	70,000
012910.14	Punto 24	100	190.61	80	2	192 x 400	70,000
012910.15	Punto 23	100	137.72	80	2	192 x 400	70,000
012910.16	Punto 24	100	190.61	90	2	192 x 400	70,000
012910.17	Punto 5	100	332.49	90	2	192 x 400	70,000
012910.18	Punto 4	100	415.39	90	2	192 x 400	70,000
012910.19	Punto 11	100	523.36	90	2	192 x 400	70,000

Table 4. Camera Frame Rates and Resolution used during the Experiment

Frame Rate fps	Maximum Resolution H x V pixels
25,000	512 x 512
50,000	192 x 512
65,100	256 x 320
75,000	192 x 312
87,500	192 x 312
100,000	192 x 264
150,000	128 x 184

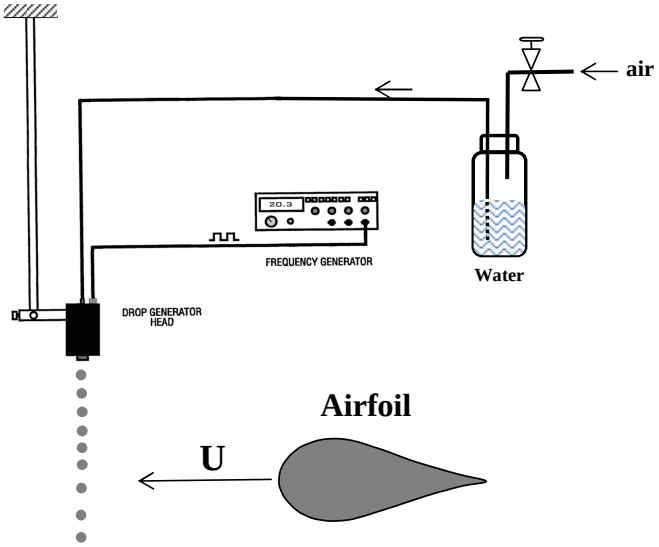

Figure 1. Conceptual View of the Experiment

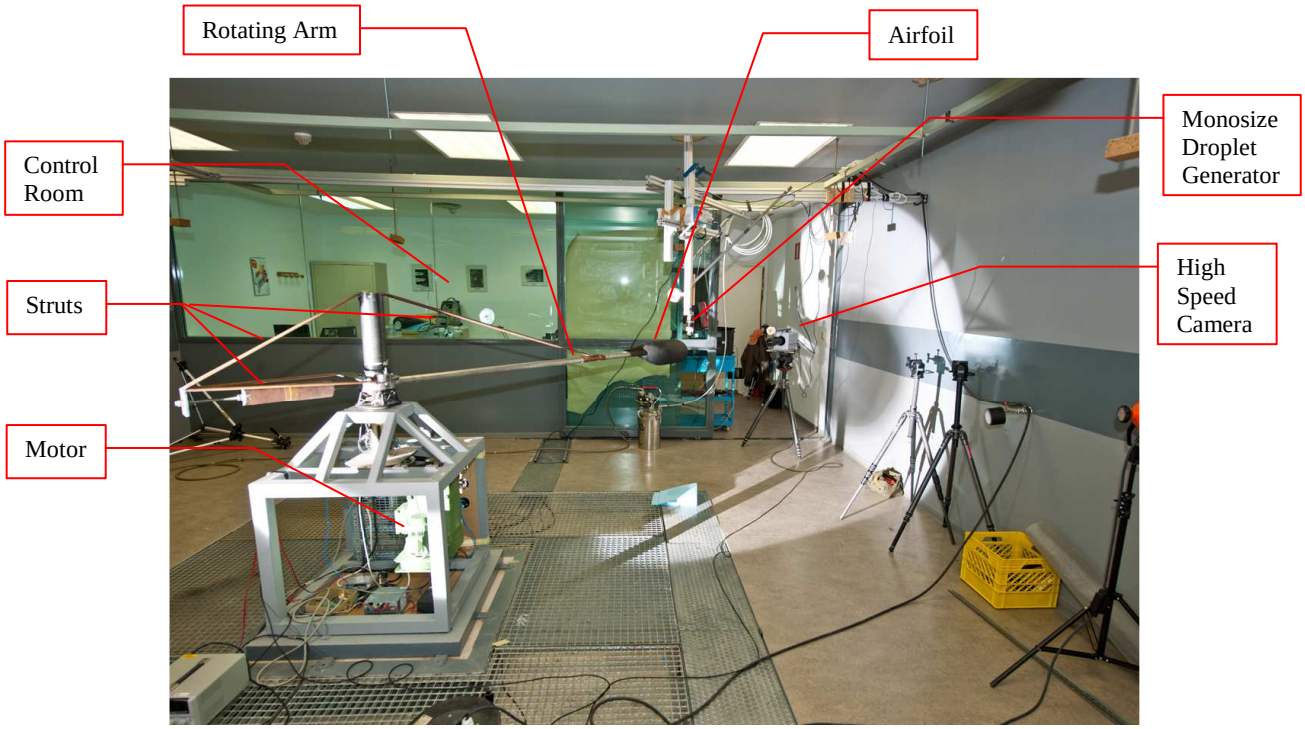

Figure 2. Experiment set-up in the INTA test cell.

(a) (b) (c)

Figure 3. DBKUP 002 Airfoil (a) Side view; (b) Front view of leading edge; (c) View from above

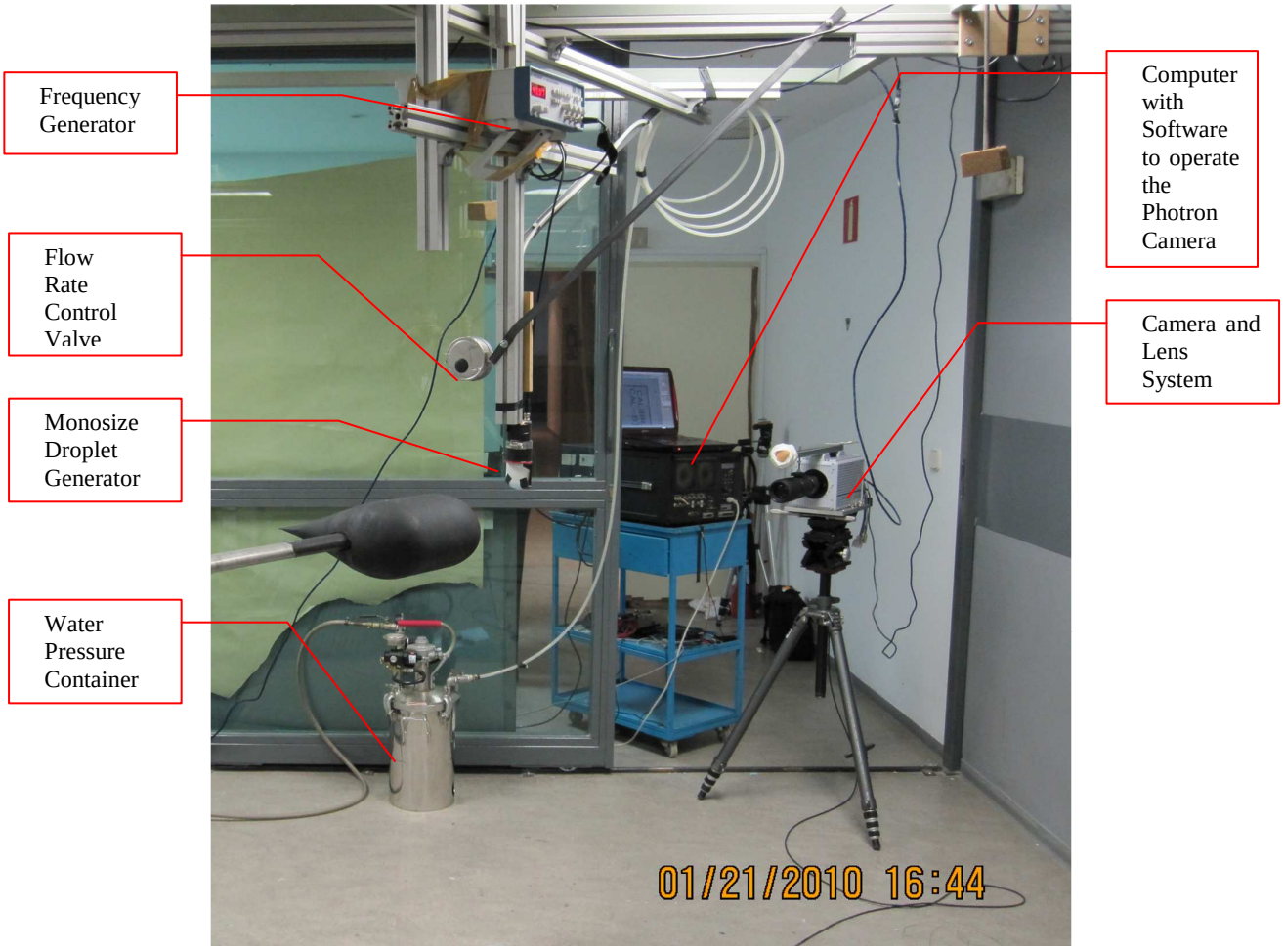

Figure 4. TSI Monosize Droplet generator, frequency generator, flow rate control valve, water pressure tank, camera and lens system, computer used to operate the camera

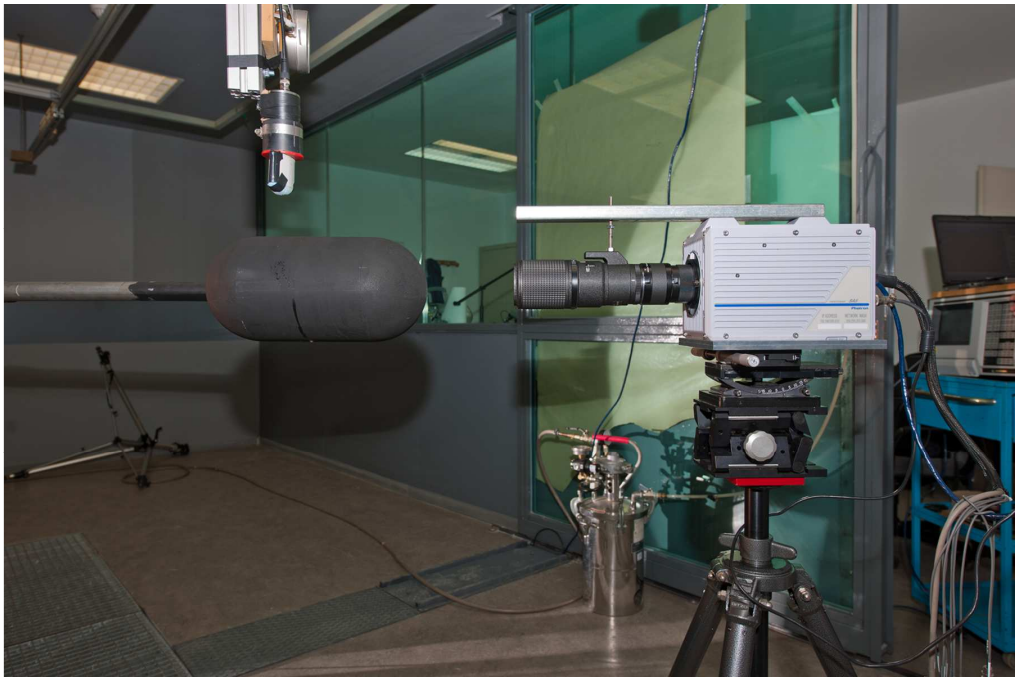

Figure 5. Close-up view of Photron SA-5 Camera with lens system. The camera is set atop an x-y positioning table. The monosize droplet generator can be observed above the airfoil

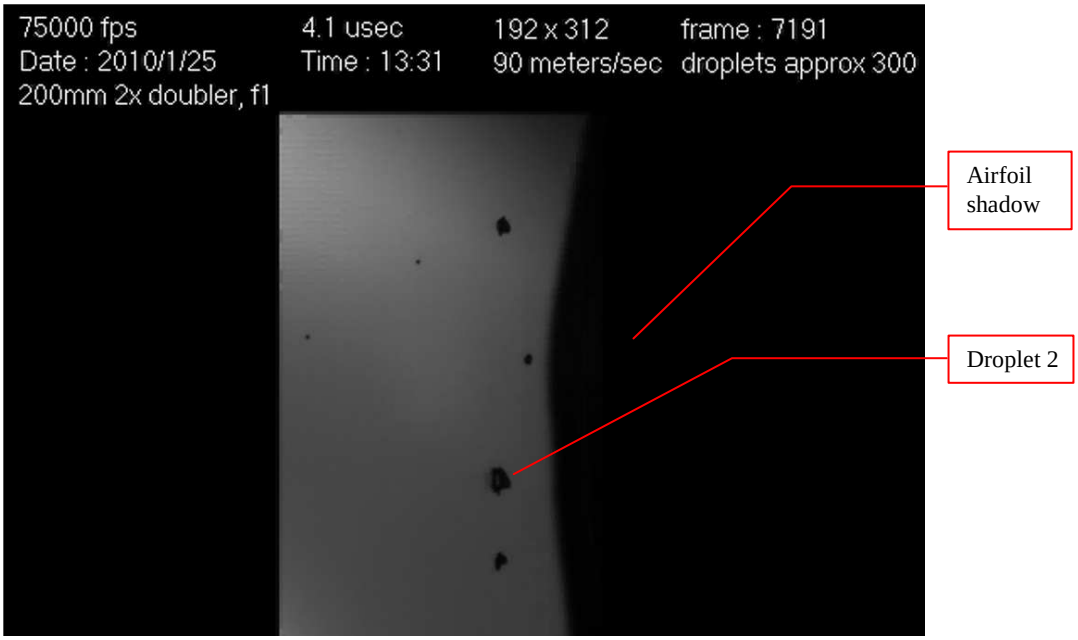

Figure 6. Documentation frame where the airfoil is about to strike the droplets. Second droplet from the bottom of the data image is labeled “droplet #2” for identification, study and tracking purposes. The droplet is in the process of breaking up. Droplet diameter = 490 mμ, Airfoil speed = 90 m/sec, camera frame rate 75,000 fps, resolution 192x312 pixels, frame 7191 Image file: 01252010-19C_Frame_7191_600dpi.tif Droplet #2

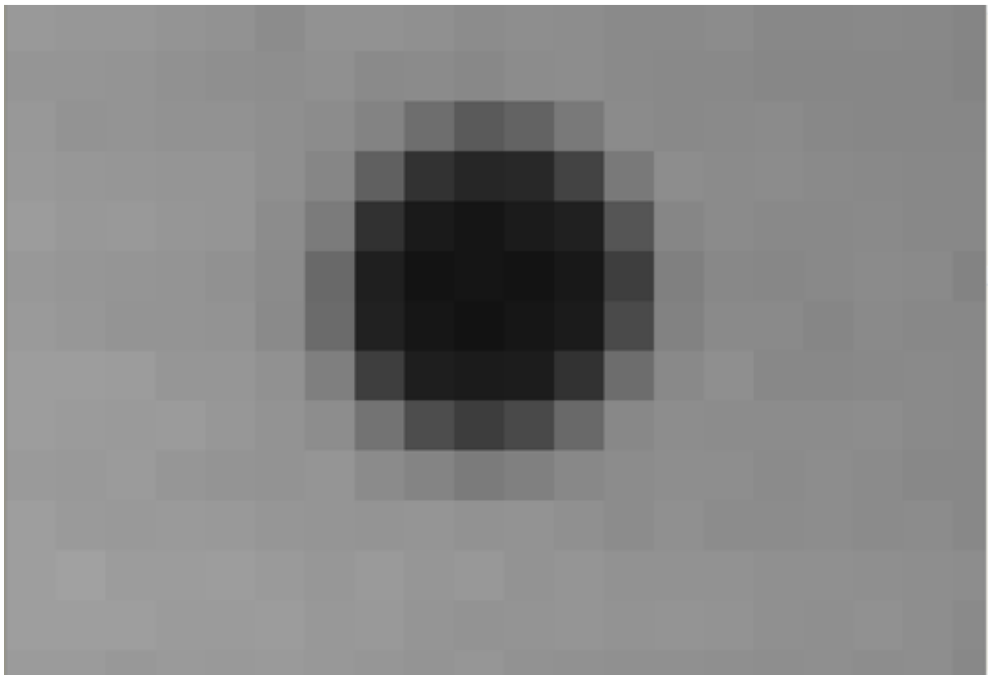

Figure 7. Zoom-in on droplet image to measure the droplet diameter. Horizontal and vertical pixels are counted and averaged out. Airfoil speed = 70 m/sec, camera frame rate 75,000 fps, resolution 192x312 pixels, frame 2175, Image 01272010-08B_Drop #2_5426_Droplet Diameter_600dpi.tif

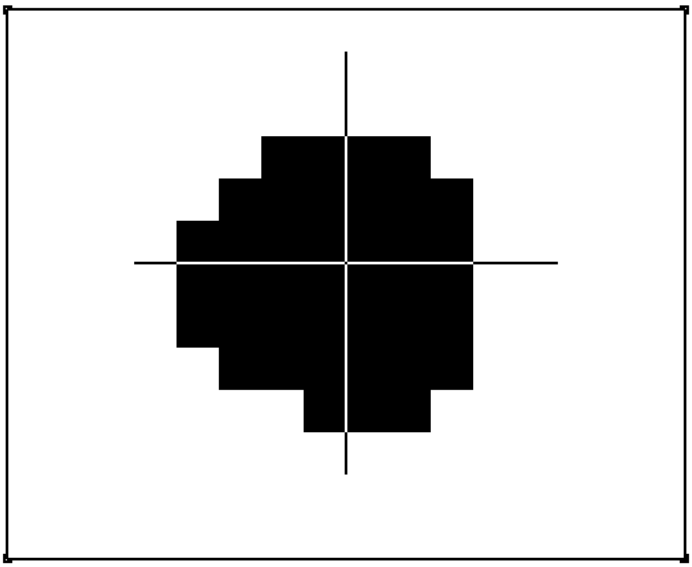

Figure 8. Threshold image of a droplet enclosed in a rectangle in preparation for continuous tracking. Airfoil speed = 50 m/sec, camera frame rate 75,000 fps, resolution 192x312 pixels, frame 2175, Image: 01252010-09_81-2098_600dpi_DropDiam.tif; Droplet #1

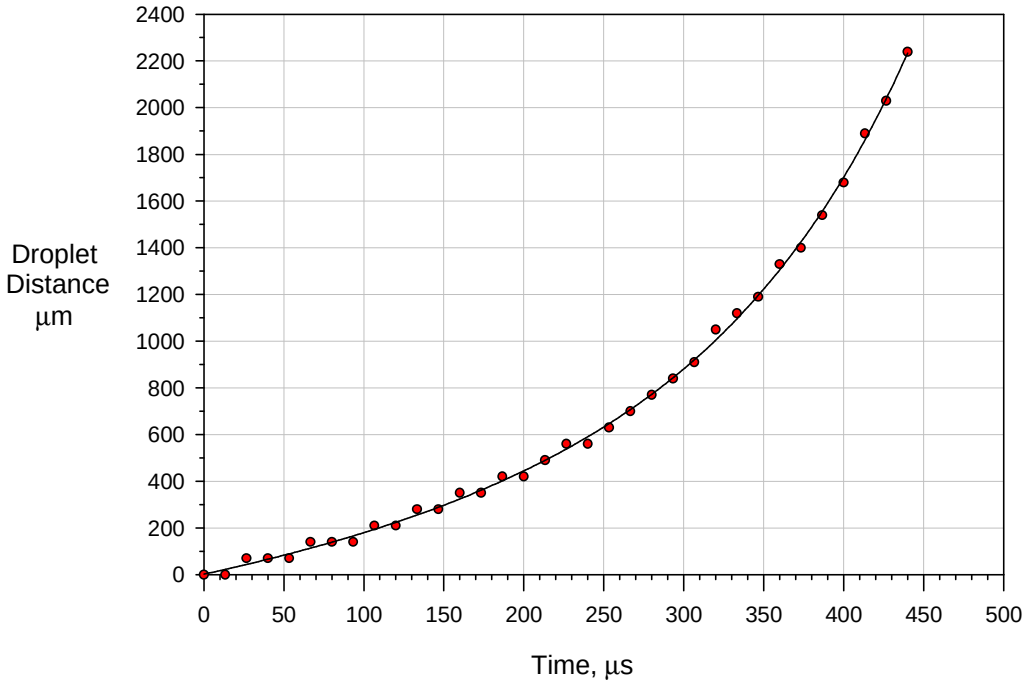

Figure 9. Horizontal displacement against time for 01252010-19C Droplet #2, Drop Diameter = 490 µm, Airfoil speed = 90 m/sec, Camera Frame Rate 75,000 fps, Resolution 192x312 pixels, Data from file: 523-50to90.xls

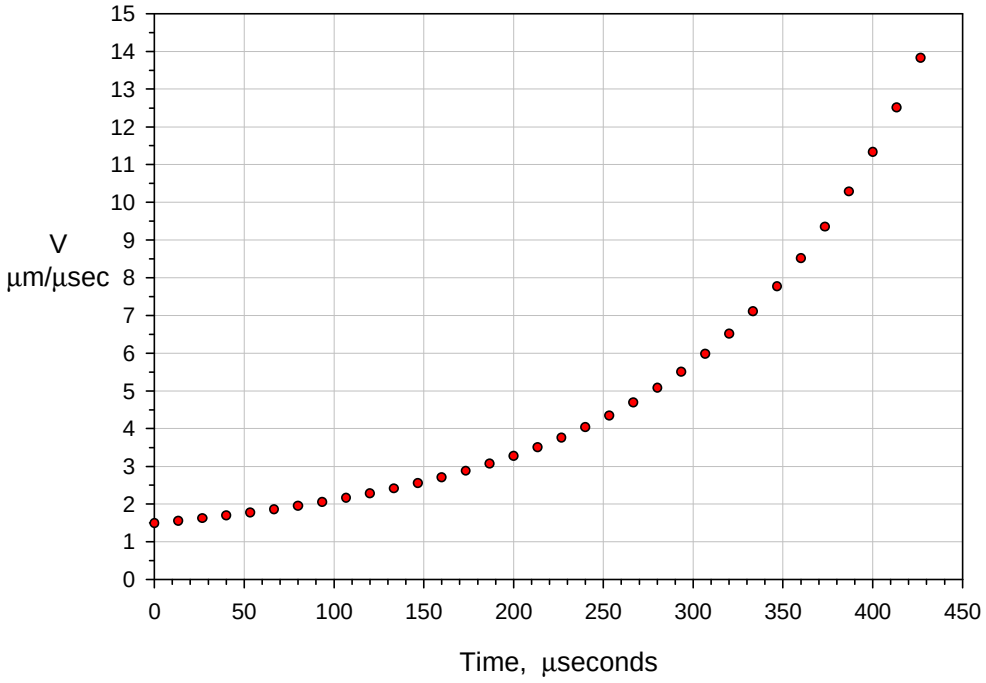

Figure 10. Horizontal velocity against time for 01252010-19C Droplet #2; Drop Diameter = 490 µm, Airfoil speed = 90 m/sec, Camera Frame Rate 75,000 fps, Resolution 192x312 pixels, Data from file: 523-50to90.xls

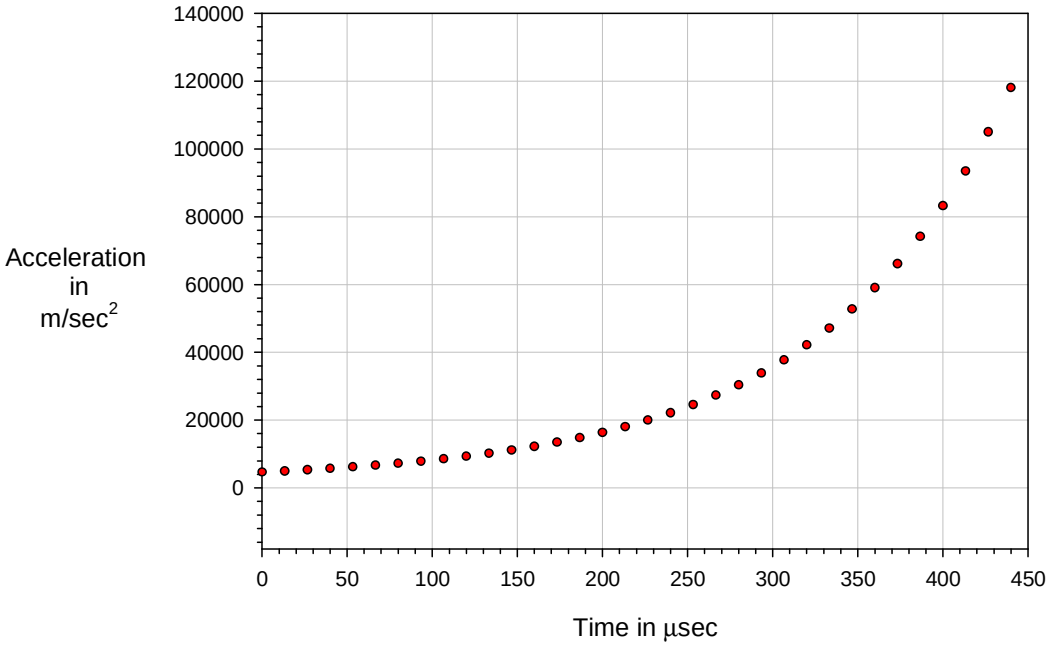

Figure 11. Horizontal acceleration against time for 01252010-19C Droplet #2, Diameter = 490 µm Airfoil speed = 90 m/sec, camera frame rate 75,000 fps, resolution 192x312 pixels, Data from file: 01252010-19C_DropletsData.xls

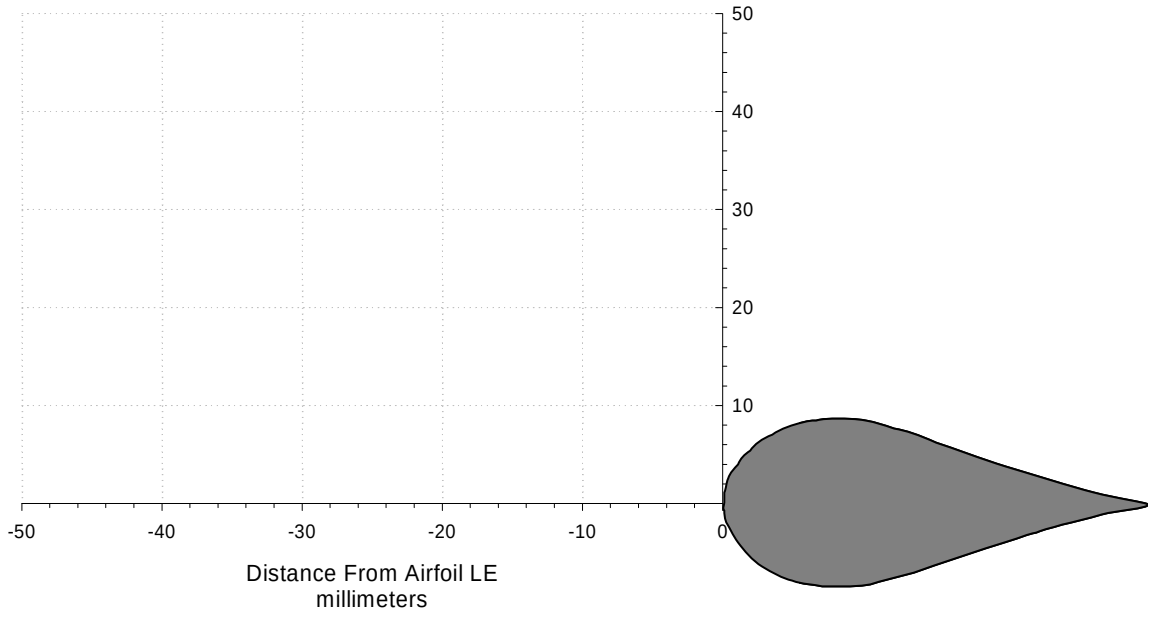

Figure 12. Frame of reference at rest with respect to the airfoil. Origin of coordinate axes located at the stagnation point of the leading edge of the airfoil. Airfoil is not drawn to scale

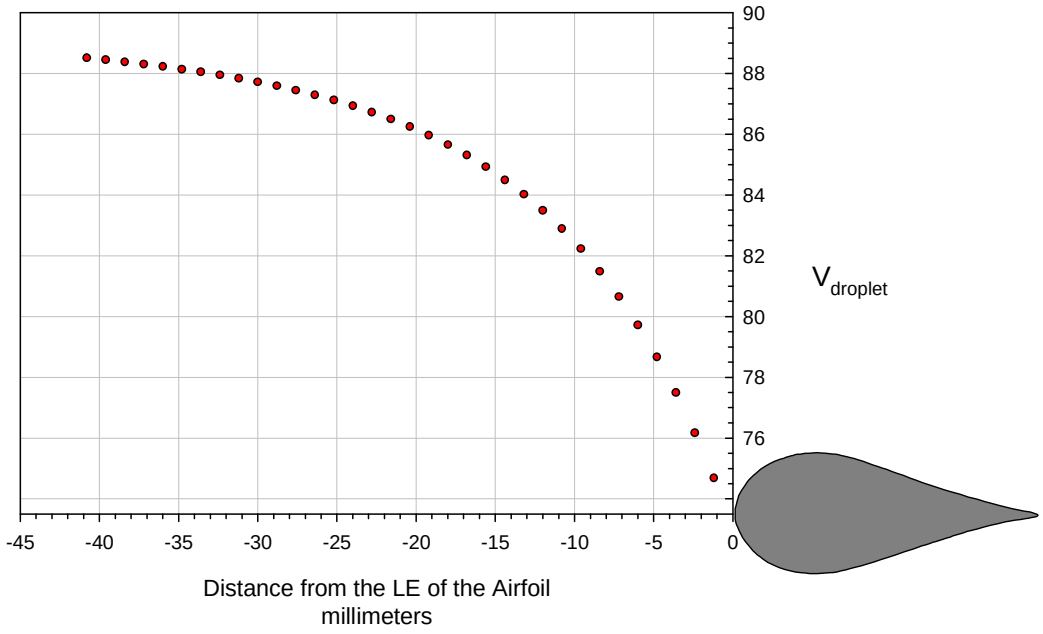

Figure 13. Droplet horizontal Velocity against Distance from the LE of the airfoil for 01252010-19C Droplet #2 Drop Diameter = 490 μm, Airfoil speed = 90 m/sec, Camera Frame Rate 75,000 fps, resolution 192x312 pixels Data from file: 523-50to90.xls

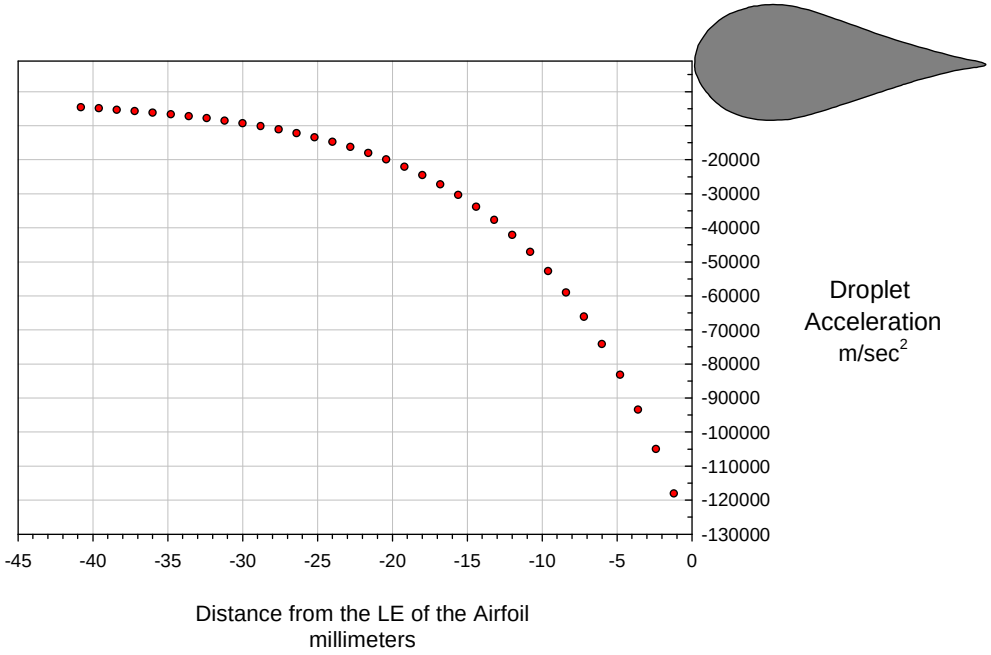

Figure 14. Droplet horizontal Acceleration against distance from the LE of the airfoil for 01252010-19C Droplet #2, Diameter = 490 μm, Airfoil speed = 90 m/sec, Camera Frame Rate 75,000 fps, Resolution 192x312 pixels Data from file: 523-50to90.xls

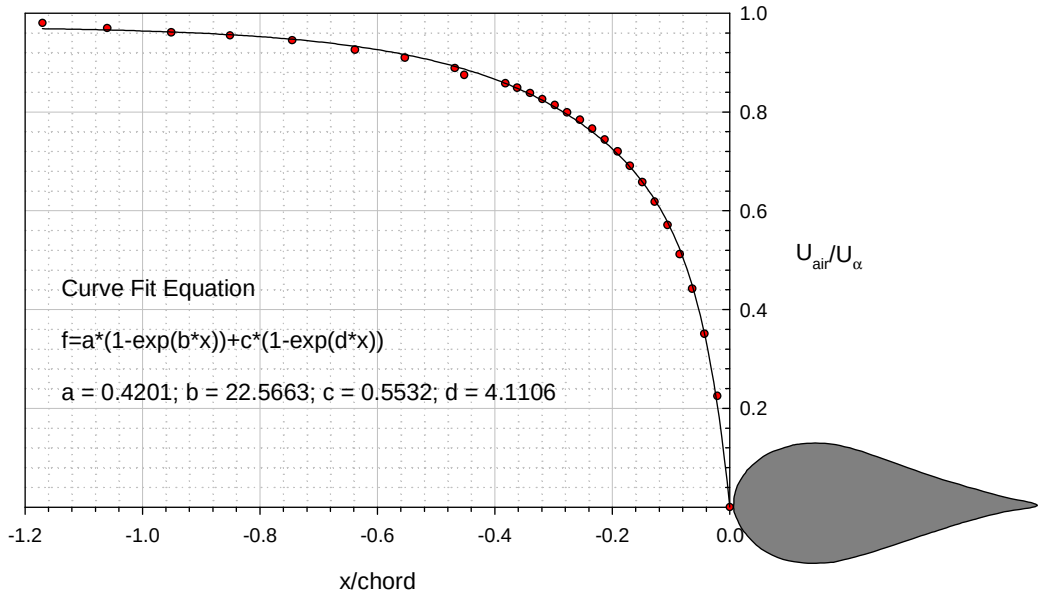

Figure 15. Experimental U_{air}/U_{α} vs. x/chord for DBKUP 002 airfoil geometry scaled down 1/10 in size, 0.047m chord Measurements conducted at the INTA 0.3m x 0.2m tunnel. Curve fit equation is shown. U_{air} is the air velocity measured with a Laser Doppler Velocimeter (LDV) at a given location along the horizontal streamline ending at the leading edge stagnation point. U_{α} is the free stream velocity.

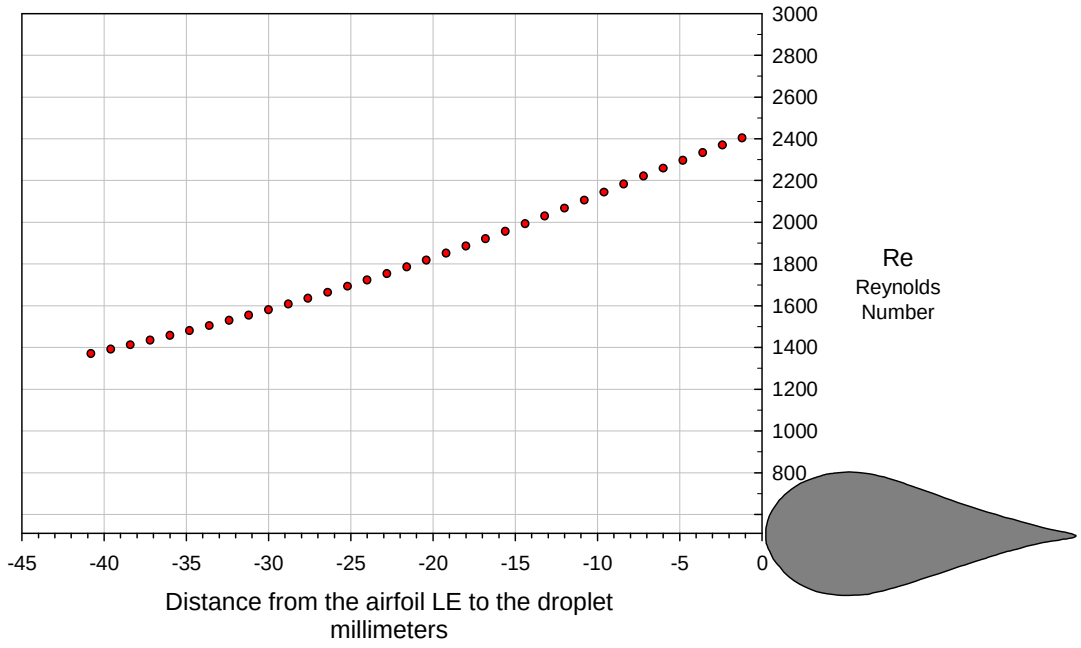

Figure 16. Reynolds number based on the calculated horizontal slip velocity and the droplet diameter for 01252010-19C Droplet #2; Drop Diameter = 490 μm, Airfoil speed = 90 m/sec, Camera Frame Rate 75,000 fps, Resolution 192x312 pixels. Data from file 523-50to90.xls

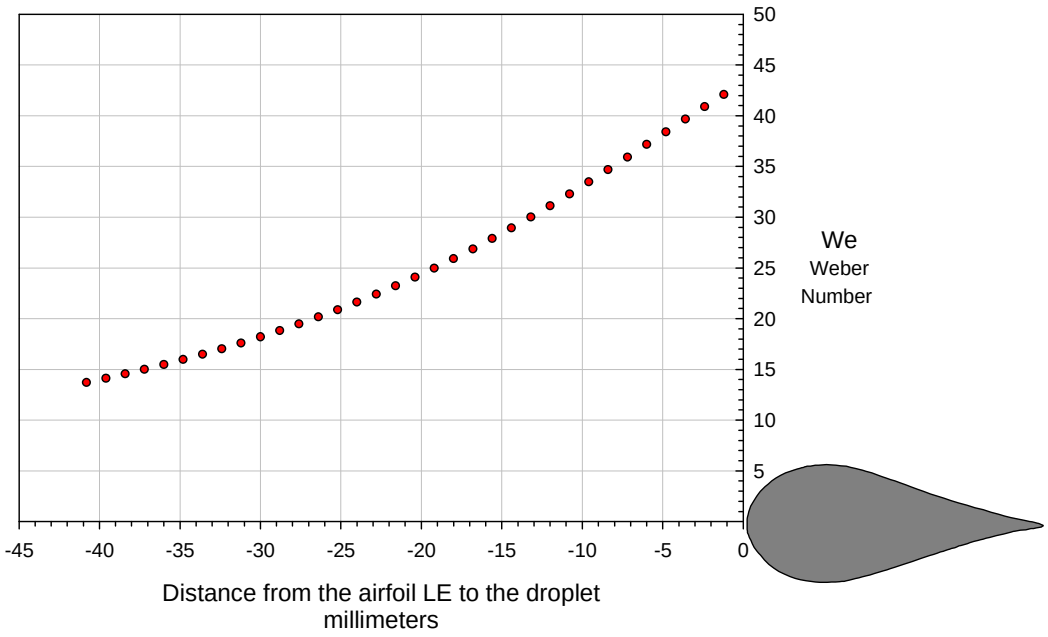

Figure 17. Weber number based on the calculated horizontal slip velocity and the droplet diameter for 01252010-19C Droplet #2; Drop Diameter = 490 μm, Airfoil speed = 90 m/sec, Camera Frame Rate 75,000 fps, Resolution 192x312 pixels

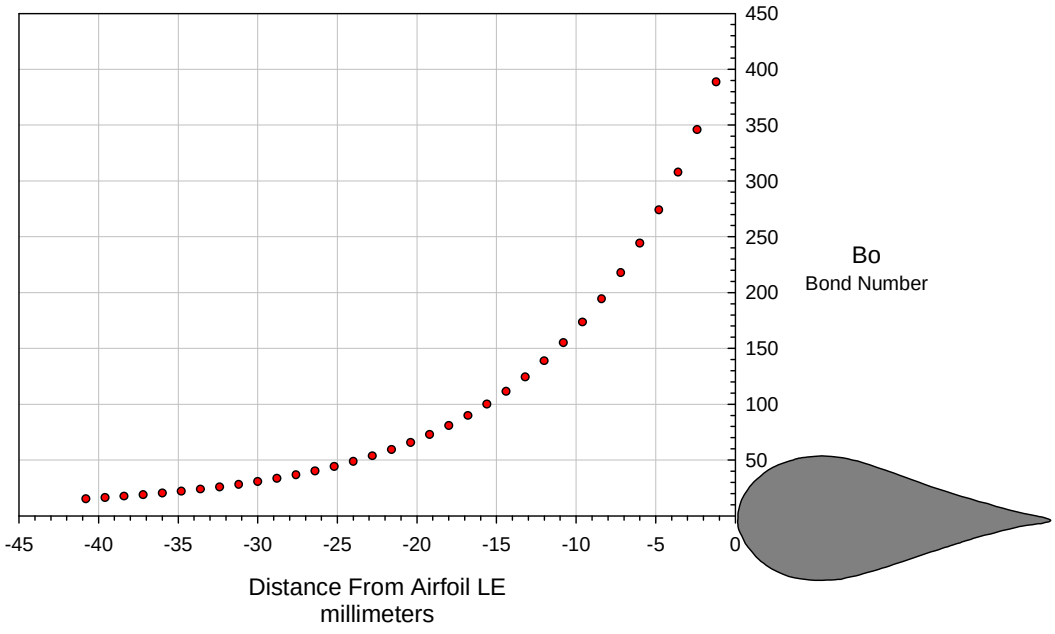

Figure 18. Bond number based on the calculated horizontal acceleration of the droplet and the droplet diameter for 01252010-19C Droplet #2; Drop Diameter = 490 μm, Airfoil speed = 90 m/sec, Camera Frame Rate 75,000 fps, Resolution 192x312 pixels

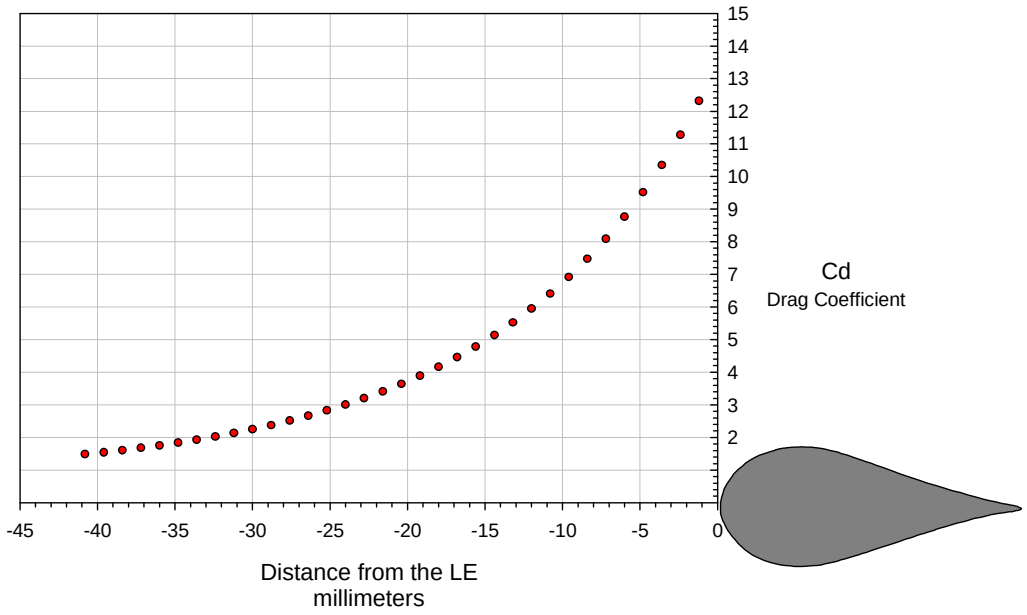

Figure 19. Drag Coefficient based on the calculated horizontal slip velocity, the acceleration and the droplet diameter for 01252010-19C Droplet #2; Drop Diameter = 490 µm, Airfoil speed = 90 m/sec, Camera Frame Rate 75,000 fps, Resolution 192x312 pixels

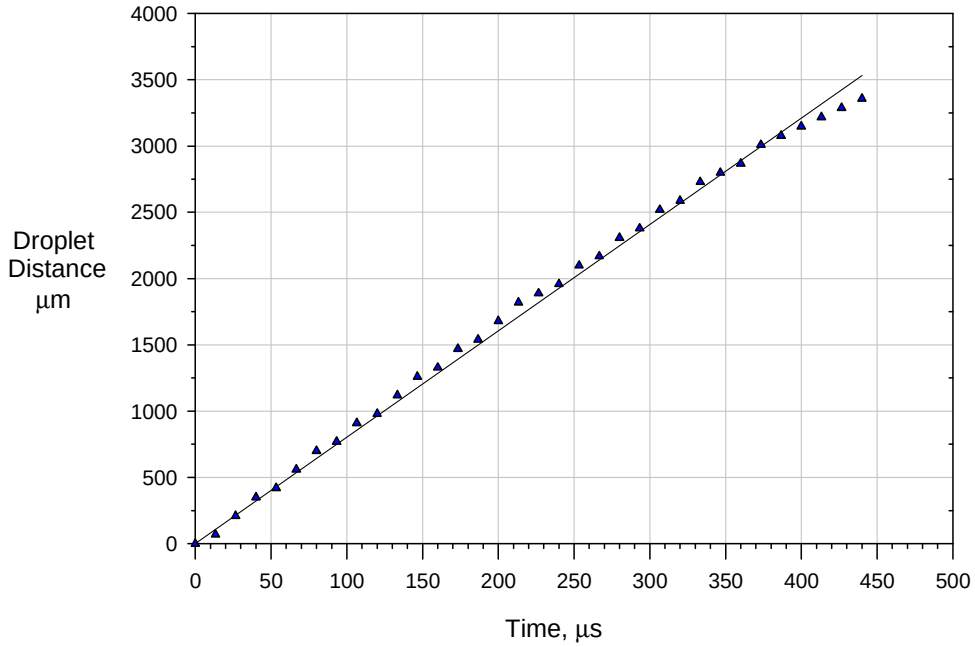

Figure 20. Vertical displacement against time for 01252010-19C Droplet #2; Drop Diameter = 490 µm, Airfoil speed = 90 m/sec, Camera Frame Rate 75,000 fps, Resolution 192x312 pixels, Data from file: 523-50to90.xls
Note: Origin of vertical axis located at the frame where the tracking of the droplet was initiated

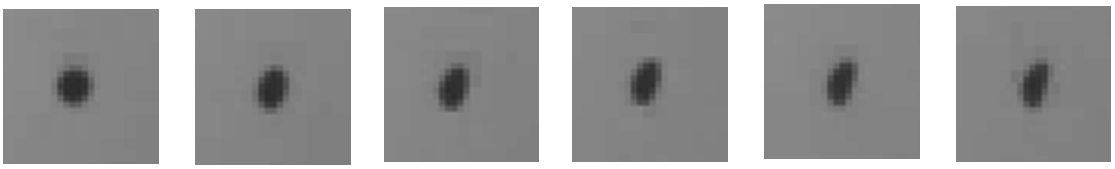

Time:	0 μsec	13.3 μsec	80.0 μsec	146.7 μsec	213.3 μsec	280.0 μsec
Distance:	81.4 mm	-69.6 mm	-63.6 mm	-57.6 mm	-51.6 mm	-45.6
We:	~ 0	7.3	8.2	9.3	10.6	12.1

Time:	346.7 μsec	413.3 μsec	480 μsec	546.7 μsec	613.3 μsec	680.0 μsec
Distance:	-39.6 mm	-33.6 mm	-27.6	-21.6	-15.6 mm	-9.6 mm
We:	14.0	16.4	19.3	23.2	28.2	34.9

Time:	706.7 μsec	733.3 μsec	760.0 μsec	786.7 μsec
Distance:	-7.2 mm	-4.8 mm	-2.4 mm	0.0 mm
We:	38.2	42.0	46.2	51.0

Figure 21. Time sequence of a droplet approaching the airfoil showing the deformation along the path. Below each droplet, the time, the distance of the droplet from the leading edge of the airfoil and the Weber number are shown. 01252010-19C Droplet #3; Drop Diameter = 490 μm, Airfoil speed = 90 m/sec, Camera Frame Rate 75,000 fps, Resolution 192x312 pixels. Frames: 140, 150, 155, 160, 165, 170, 175, 180, 185, 190, 195, 200, 202, 204, 206 and 208

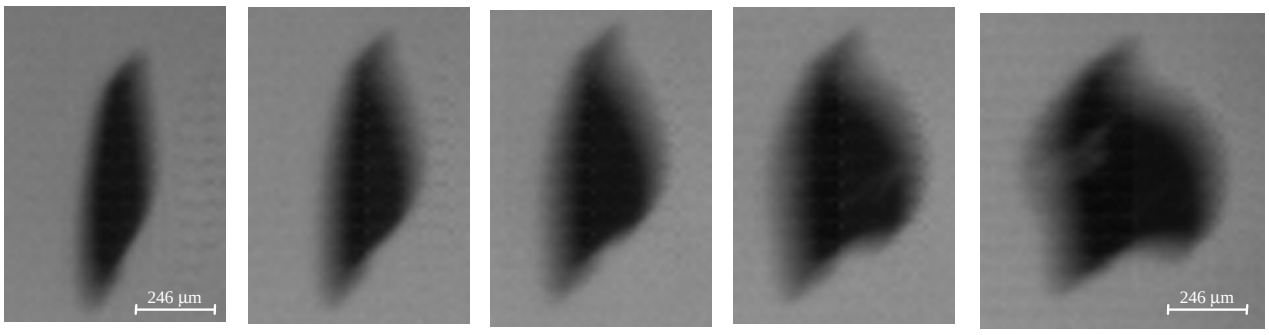

t = 0 µsec	t = 57.1 µsec	t = 85.7 µsec	t = 114.3 µsec	t = 142.9 µsec
15.5 mm	10.3 mm	7.7 mm	5.2 mm	2.6 mm

Figure 22. Time sequence of the later stages of the droplet breakup. The "bag" type of breakup can be observed. The distance scale is shown on the first and last images (246µm). The time from the first frame to breakup is indicated below each image. The distance from the leading edge of the airfoil is indicated below the time. Movie 01292010-11D droplet #1; Airfoil speed = 90 m/sec, Camera Frame Rate 70,000 fps, Resolution 192x400 pixels

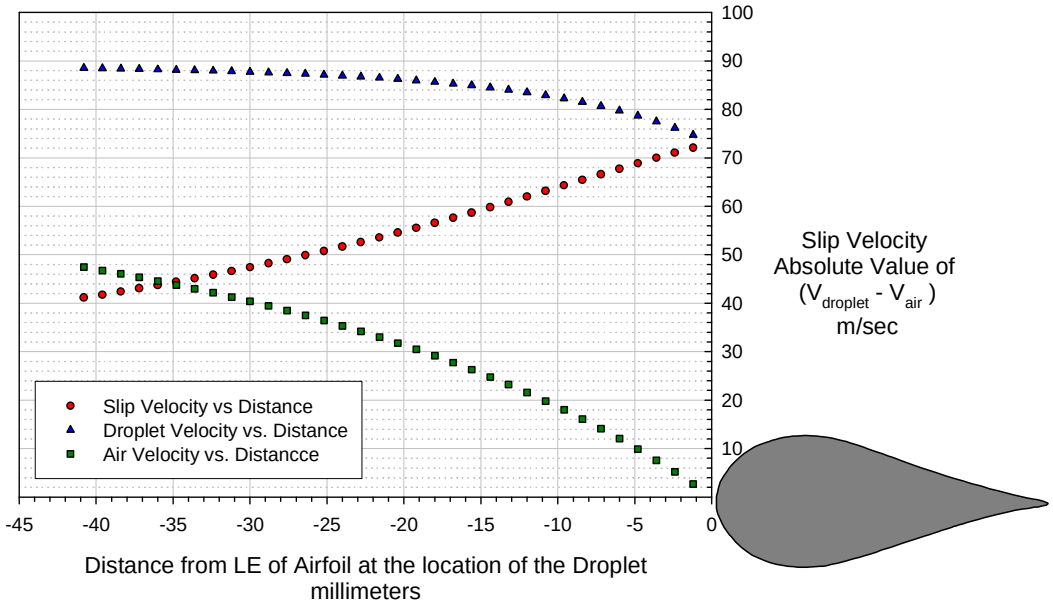

Figure 23. Droplet velocity, air velocity and slip velocity for 01252010-19C Droplet #2; Drop Diameter = 490 µm, Airfoil speed = 90 m/sec, Camera Frame Rate 75,000 fps, Resolution 192x312 pixels

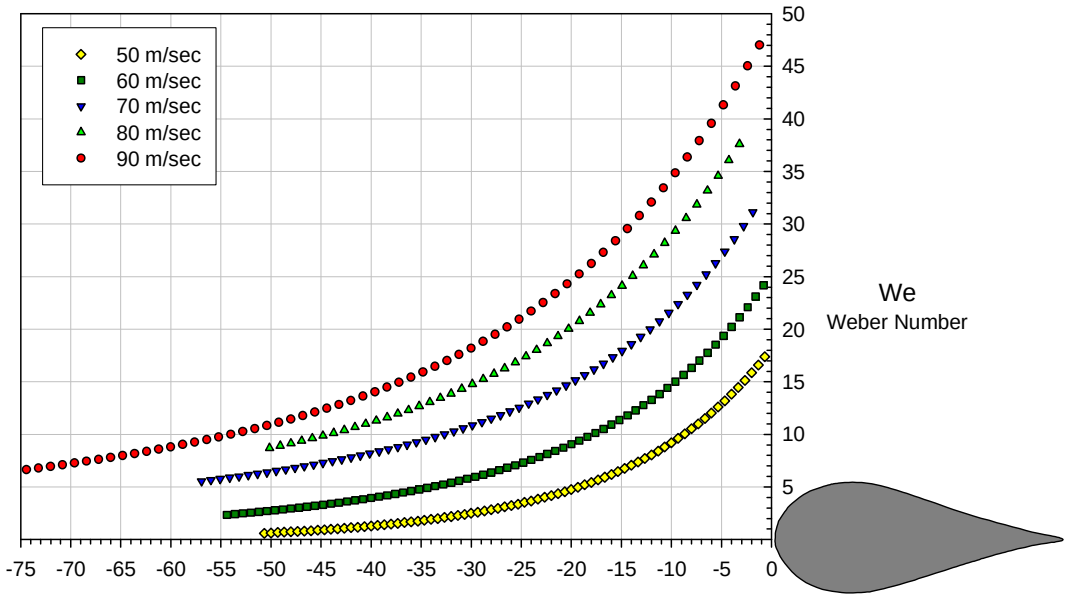

Figure 24. Weber Number against distance from the leading edge of the airfoil for droplets of 490 µm at each velocity of 50 to 90 m/sec. Camera Frame Rate 75,000 fps, Resolution 192x312 pixels

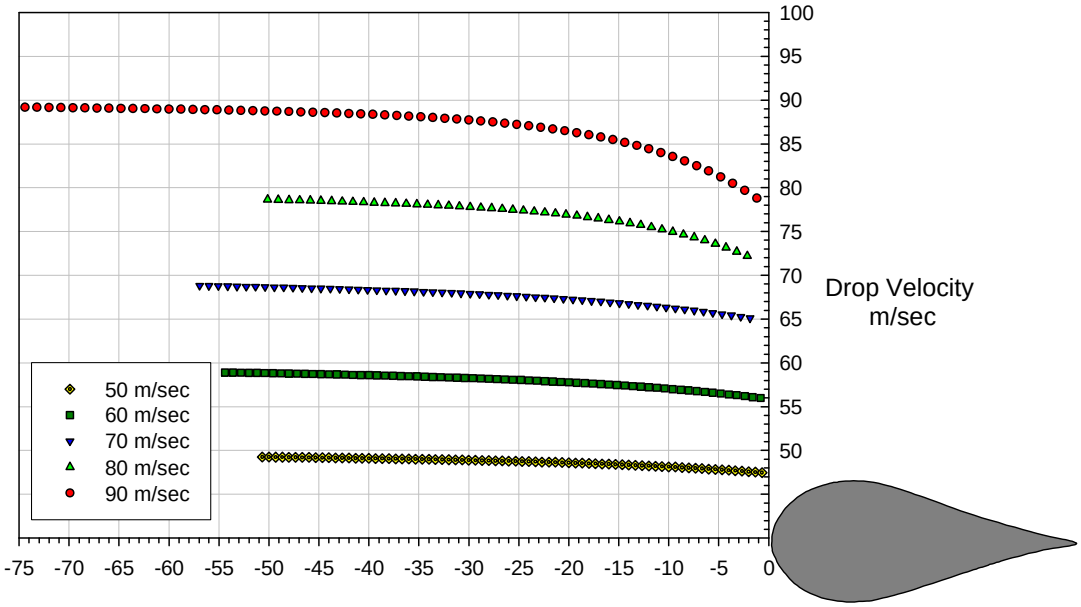

Figure 25. Drop velocities against distance from the leading edge of the airfoil for droplets of 490 µm at each velocity of 50 to 90 m/sec. Camera Frame Rate 75,000 fps, Resolution 192x312 pixels

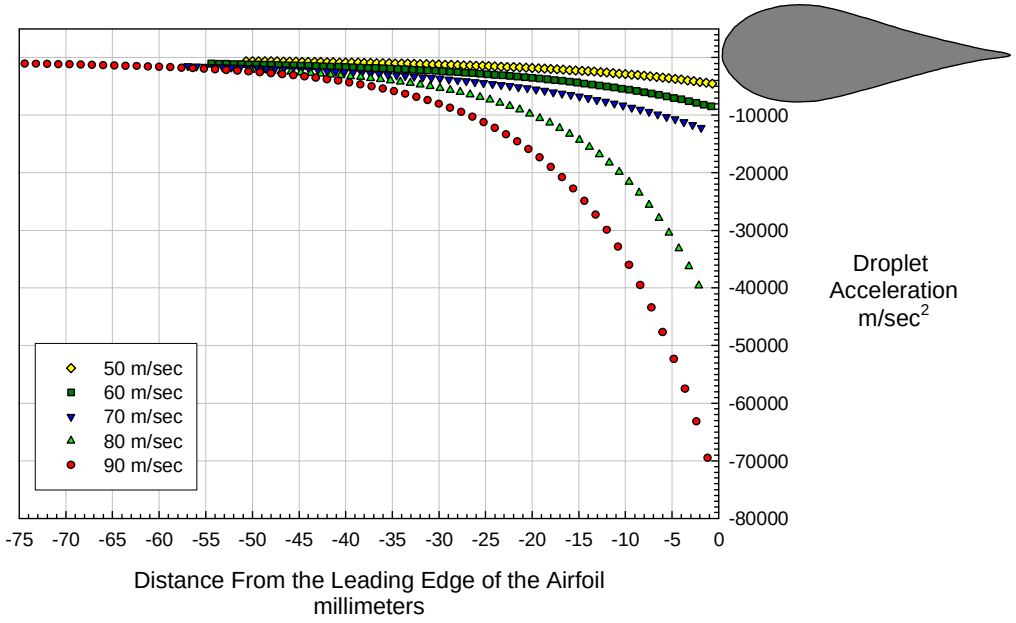

Figure 26. Droplet acceleration against distance from the leading edge of the airfoil for droplets of 490 µm at each velocity of 50 to 90 m/sec. The acceleration is in the opposite direction from the motion of the droplet (deceleration). Camera Frame Rate 75,000 fps, Resolution 192x312 pixels

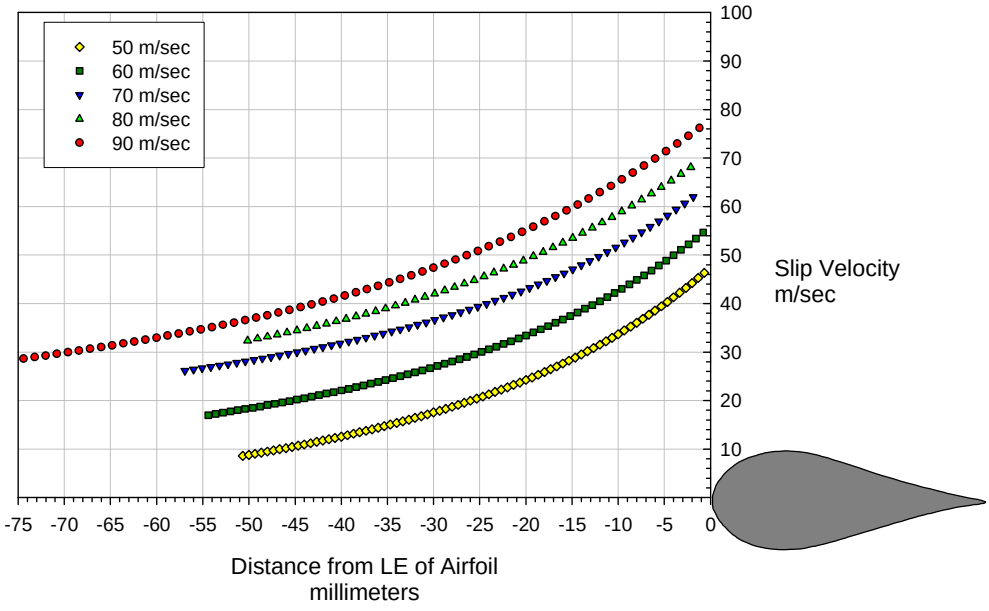

Figure 27. Slip velocity against distance from the leading edge of the airfoil for droplets of 490 µm at each velocity of 50 to 90 m/sec. Camera Frame Rate 75,000 fps, Resolution 192x312 pixels

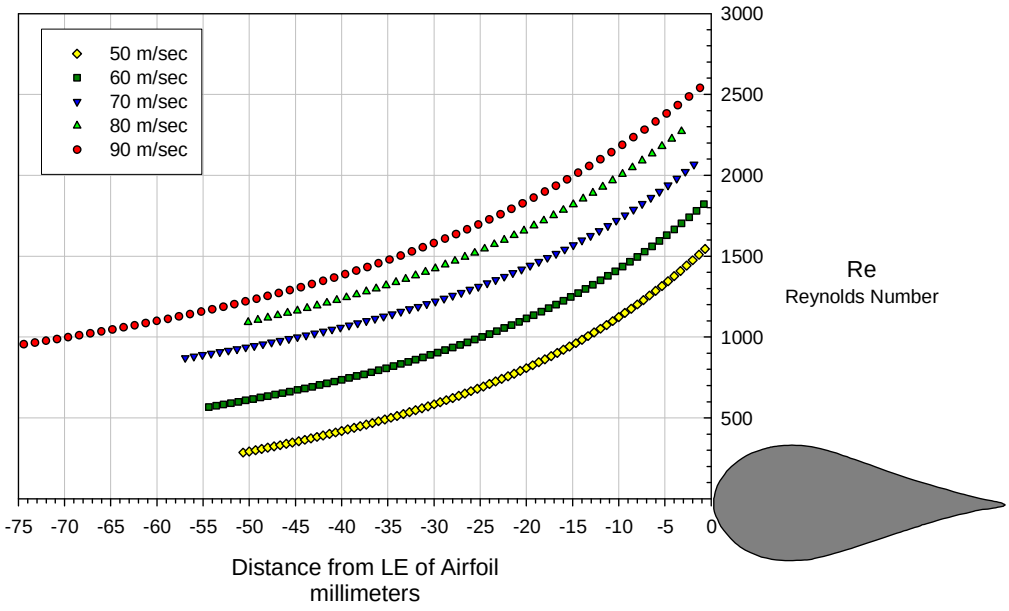

Figure 28. Reynolds number against distance from the leading edge of the airfoil for droplets of 490 µm at each velocity of 50 to 90 m/sec. Camera Frame Rate 75,000 fps, Resolution 192x312 pixels

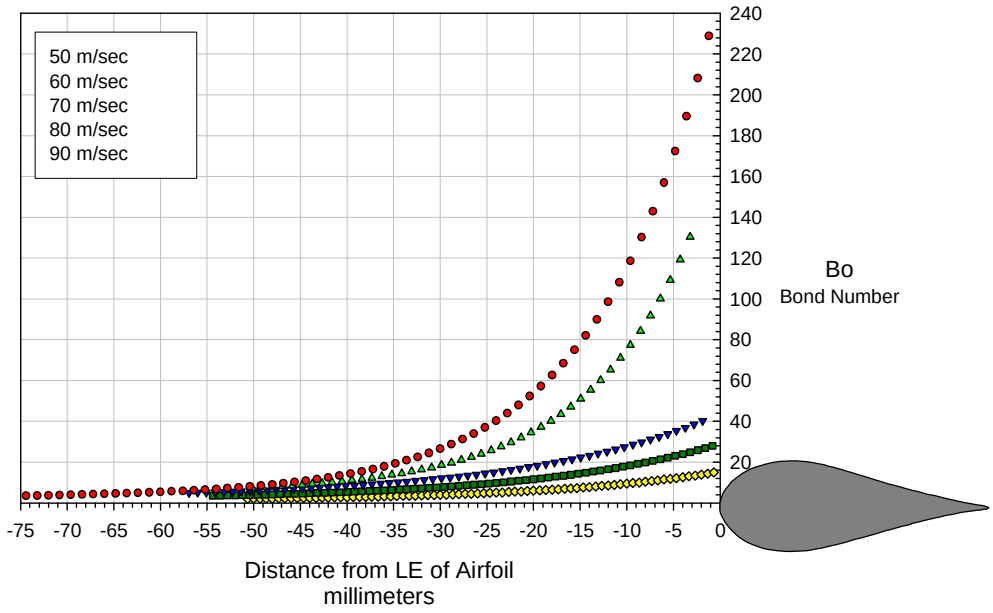

Figure 29. Bond Number against distance from the leading edge of the airfoil for droplets of 490 µm at each velocity of 50 to 90 m/sec. Camera Frame Rate 75,000 fps, Resolution 192x312 pixels

REPORT DOCUMENTATION PAGE	Form Approved OMB No. 0704-0188

1. REPORT DATE *(DD-MM-YYYY)*	2. REPORT TYPE	3. DATES COVERED *(From - To)*
01-01-2011	Technical Memorandum	

4. TITLE AND SUBTITLE
Experimental Observations on the Deformation and Breakup of Water Droplets Near the Leading Edge of an Airfoil

5a. CONTRACT NUMBER

5b. GRANT NUMBER

5c. PROGRAM ELEMENT NUMBER

6. AUTHOR(S)
Vargas, Mario; Feo, Alex

5d. PROJECT NUMBER

5e. TASK NUMBER

5f. WORK UNIT NUMBER
WBS 457280.02.07.03.02

7. PERFORMING ORGANIZATION NAME(S) AND ADDRESS(ES)
National Aeronautics and Space Administration
John H. Glenn Research Center at Lewis Field
Cleveland, Ohio 44135-3191

8. PERFORMING ORGANIZATION REPORT NUMBER
E-17550

9. SPONSORING/MONITORING AGENCY NAME(S) AND ADDRESS(ES)
National Aeronautics and Space Administration
Washington, DC 20546-0001

10. SPONSORING/MONITOR'S ACRONYM(S)
NASA

11. SPONSORING/MONITORING REPORT NUMBER
NASA/TM-2011-216946

12. DISTRIBUTION/AVAILABILITY STATEMENT
Unclassified-Unlimited
Subject Categories: 01, 03, 31 and 34
Available electronically at http://www.sti.nasa.gov
This publication is available from the NASA Center for AeroSpace Information, 443-757-5802

13. SUPPLEMENTARY NOTES

14. ABSTRACT
This work presents the results of an experimental study on droplet deformation and breakup near the leading edge of an airfoil. The experiment was conducted in the rotating rig test cell at the Instituto Nacional de Técnica Aeroespacial (INTA) in Madrid, Spain. An airfoil model placed at the end of the rotating arm was moved at speeds of 50 to 90 m/sec. A monosize droplet generator was employed to produce droplets that were allowed to fall from above, perpendicular to the path of the airfoil at a given location. High speed imaging was employed to observe the interaction between the droplets and the airfoil. The high speed imaging allowed observation of droplet deformation and breakup as the droplet approached the airfoil near the stagnation line. A tracking software program was used to measure from the high speed movies the horizontal and vertical displacement of the droplet against time. The velocity, acceleration, Weber number, Bond number, Reynolds number, and the drag coefficients were calculated along the path of a given droplet from beginning of deformation to breakup and/or hitting the airfoil. Results are presented for droplets with a diameter of 490 micrometers at airfoil speeds of 50, 60, 70, 80 and 90 m/sec.

15. SUBJECT TERMS
Droplet breakup; Supercooled large droplet icing (SLD); Icing

16. SECURITY CLASSIFICATION OF:			17. LIMITATION OF ABSTRACT	18. NUMBER OF PAGES	19a. NAME OF RESPONSIBLE PERSON
a. REPORT	b. ABSTRACT	c. THIS PAGE			STI Help Desk (email:help@sti.nasa.gov)
U	U	U	UU	40	19b. TELEPHONE NUMBER *(include area code)* 443-757-5802